NRC/USGS Workshop Report: Landslide Tsunami Probability

Project Title: Tsunami Landslide Source Probability and Potential Impact on New and Existing Power Plants (JCN V6166)

By Eric L. Geist and Uri S. ten Brink

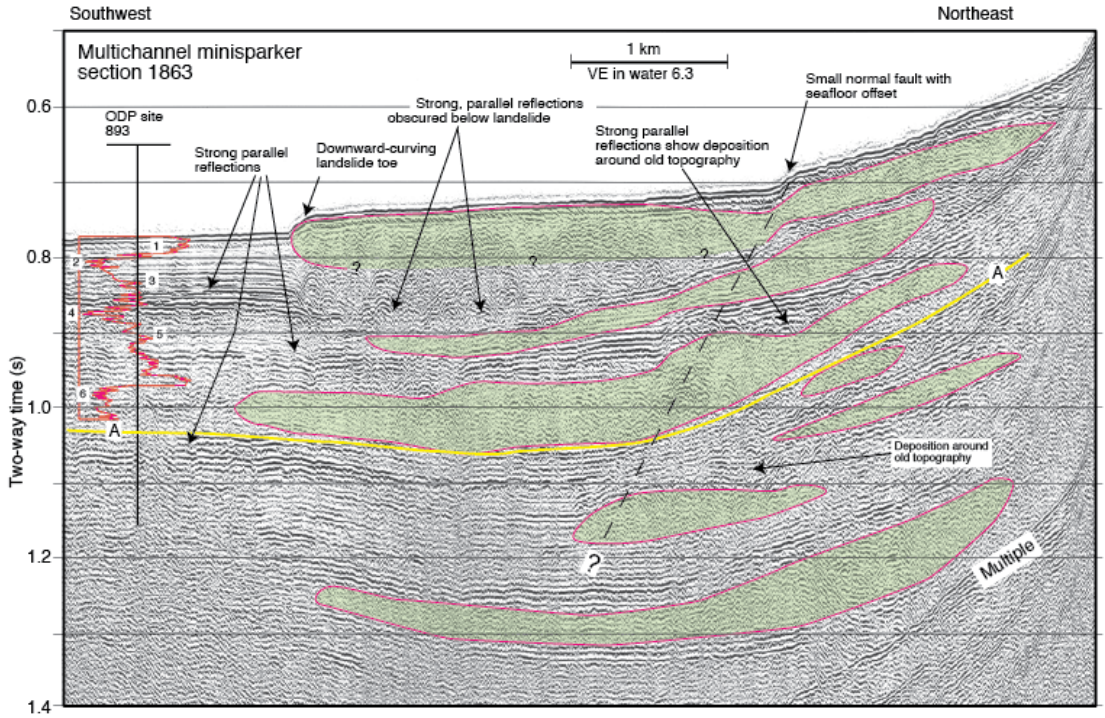

Administrative Report, 2012

U.S. Department of the Interior
U.S. Geological Survey

Table of Contents

Cover: High-resolution minisparker seismic reflection data oriented parallel to the axis of the Goleta (California) landslide complex. Red outline and green shading indicates interpreted landslide deposits. Red curve is the oxygen isotope variation from ODP site 893. Numbers represent marine isotope stages. Figure from Fisher and others (2005).

Introduction

A Nuclear Regulatory Commission (NRC) sponsored workshop entitled "NRC/USGS Workshop on Landslide Probability" was held on August 18-19 at the U.S. Geological Survey (USGS) Woods Hole Science Center in Woods Hole, Massachusetts. Academic, industry, and government participants provided an overview of topics that included geological characterization of submarine landslides, geotechnical techniques and measurements of slope stability, hydrodynamic modeling of landslide-generated tsunamis, and probabilistic methods for hazard assessment. The goal of the workshop was to bring together experts who study the geometry and recurrence of slope failures, their geotechnical properties, their potential tsunami generation, and the probability of recurrence of extreme events, to answer the following questions:

A) Using current data, what can we say about the probability for submarine mass failures?

B) How do we treat the dynamics of landslide movement probabilistically?

C) How do we treat propagation and runup of tsunami waves probabilistically?

D) What new probabilistic methods can be developed specifically for submarine mass failures?

Although probability is mentioned in all of these questions, a probabilistic assessment is only as good as the underlying data and assumptions; therefore, it is critical that we address the state of knowledge and the kinds of new data that needs to be collected to improve our ability to estimate probability of occurrence.

Currently, tsunami hazards are evaluated by the NRC for new license applications in terms of determining the probable maximum tsunami (PMT) defined as (González and others, 2007; Prasad, 2009):

> *...that tsunami for which the impact at the site is derived from the use of best available scientific information to arrive at a set of scenarios reasonably expected to affect the nuclear power plant site, taking into account (1) appropriate consideration of the most severe of the natural phenomena that have been historically reported for the site and surrounding area, with sufficient margin for the limited accuracy, quantity, and period of time in which the historical data have been accumulated; (2) appropriate combinations of the effects of normal and accident conditions with the effects of the natural phenomena; and (3) the importance of the safety functions to be performed.*

In contrast, seismic hazards are evaluated by the NRC in terms of probabilistic methods (Senior Seismic Hazard Analysis Committee, 1997). There is ongoing research to explore whether tsunami hazards can be evaluated at design probabilities of interest to the NRC using probabilistic tsunami hazard analysis (PTHA). PTHA is closely akin to probabilistic seismic hazard analysis (PSHA) (Cornell, 1968; Senior Seismic Hazard Analysis Committee, 1997). A primary difference between PTHA and PSHA is that numerical propagation models can be used for tsunamis in place of seismic attenuation

relations (Geist and Parsons, 2006; Geist and others, 2009b). The distinct disadvantage of PTHA at very low probabilities, such as for nuclear power plant applications, is the need to include submarine landslides in the analysis. Recurrence information for submarine landslides is uncertain or altogether lacking in some regions, resulting high uncertainty in the source term for probabilistic analysis, compared to earthquake recurrence.

For the last several years, the USGS has done research to identify and date significant submarine landslides along the western Atlantic margin of the U.S. and the Gulf of Mexico (ten Brink and others, 2009a). Recent efforts have focused on how submarine landslide probability might be determined using available geological and geophysical information and identifying the challenges of incorporating this information into PTHA. Much of the research to date is described in this report, culminating in the August 2011 Woods Hole workshop that highlighted current research from academic, industry, and government scientists in the U.S.

Pre-Workshop Research

Prior to the workshop, information was gathered related to the theoretical background for determining submarine landslide probability and incorporation of landslides into PTHA. This information is presented below, divided into the general probabilistic framework of PTHA, submarine landslide dynamics as it relates to tsunami generation, and probabilistic approaches for determining landslide rates. Included after these sections are specific challenges related to determining submarine landslide probability and its inclusion into PTHA, as well as a section on potential future science directions.

Workshop Presentations

The abstracts and presentations that were given at the workshop are included in the appendix of this report. The presentations were grouped into four sessions: (1) landslide geometry and recurrence; (2) landslide mechanics; (3) modeling landslide tsunamis; and (4) probability of landslides and landslide tsunamis.

The landslide geometry and recurrence session included an overview talk on how submarine landslides are identified, including potential pitfalls (Lee presentation) and an overview of mapped landslides in the Gulf of Mexico and U.S. Atlantic margins (Twichell presentation). Details of various techniques used to date submarine landslides and sediment transport processes associated with landslides were given in the Chaytor and Brothers presentations, respectively.

The first three talks in the landslide mechanics session focused on geotechnical characterization of slope stability, including a technique for determining landslide occurrence given information on earthquake ground-shaking probabilities and bathymetric slope (ten Brink presentation). The DeGroot presentation provided specific information on state-of-the art instrumentation to provide geotechnical characterization of the seafloor. An overview of geotechnical considerations for landslide occurrence was provided in the Locat presentation, followed by a presentation of a newly-developed numerical model for simulating landslide dynamics (George presentation).

The modeling landslide tsunamis session focused on state-of-the art hydrodynamic modeling of long- and intermediate-length waves associated with this

unique type of tsunami. Conventional 2-horizontal dimension (2HD) models were compared with 3D models in the Horrillo presentation and laboratory experiments used to validate hydrodynamic models were described in the Grilli presentation. In the Lynett presentation, non-linear Boussinesq-type models were used to show how probabilistic variations in down-slope landslide length can be evaluated. For the final presentation in this session, González showed how numerical hydrodynamic models are used in PTHA, providing a transition to the final session of the workshop.

The probability of landslides and landslide tsunamis session began with a presentation of how PTHA has been applied in the Pacific Basin and how disaggregation can provide important information about which source regions dominate the probabilistic calculations (Thio presentation). A version of PTHA specific to submarine landslides was presented by Baxter, in which geotechnical calculations were combined with tsunami-scaling relations for the U.S. east coast to estimate tsunami hazards. A method to determine landslide probabilities over a broad region by using seafloor databases, such as usSEABED, was presented by Morgan. Results of the workshop were synthesized into a presentation about the approaches and challenges of incorporating submarine landslides into PTHA (Geist presentation).

The workshop presentations provided a sampling of current thinking related to submarine landslides, their probability, and the complex hydrodynamics of landslide tsunamis. Details of each presentation are provided in the appendix.

General Probabilistic Framework

Probabilistic Tsunami Hazard Analysis (PTHA) is derived directly from Probabilistic Seismic Hazard Analysis (PSHA) developed by Allin Cornell in 1968 (Cornell, 1968). PTHA calculates the rate of tsunamis exceeding a particular runup value at a particular location at the coastline, given by

$$\lambda\left(R > R_0\right).$$

The rate is used in the calculation of Poisson probabilities, and it typically is assumed that the rate does not change with time. The probability (P) over T years that runup will be exceeded is given by

$$P\left(R > R_0\right) = 1 - \exp(-\lambda \mathrm{T}).$$

Both PSHA and PTHA includes three steps:
(1) Define source parameters, including source probabilities, for all relevant sources.
(2) Calculate wave heights from a generation and propagation model for each source.
(3) Aggregate the results to determine the tsunami hazard curve for a particular coastal site.

Probabilistic Seismic Hazard Analysis Equation

The PSHA framework equation to determine the rate of ground motion exceedance ($A > A_0$) for multiple-source locations indexed by i is given by (Senior Seismic Hazard Analysis Committee, 1997)

$$\lambda\left(A > A_0\right) = \sum_i^S \nu_i \int\int \Phi\left(\frac{\ln A - g(m,r)}{\sigma}\right) f(m) f(r|m) dr dm$$

In the above equation, *r* is the distance from the source to the site,

$$\nu_i$$

is the mean rate of occurrence of all earthquakes at location *i*, *f(m)* is the probability density function (pdf) for magnitude, and *f(r|m)* is the pdf for distance for a given magnitude.

$$\Phi\left(\frac{\ln A - g(m,r)}{\sigma}\right)$$

is the complementary cumulative distribution function for the ground-motion attenuation relationship, dependent on magnitude and distance.

Probabilistic Tsunami Hazard Analysis Equation (Continuously Distributed Sources)

The PTHA framework equation for multiple tsunami sources is related to the PSHA equation, except that multiple types of sources are involved and that the ground-motion attenuation relationship is substituted with numerical tsunami generation and propagations. The PTHA equation for continuously distributed sources is given by (Geist and others, 2009b)

$$\lambda\left(R > R_0\right) = \sum_{\text{type}=i} \nu_i \int\int P\left(R > R_0 | \psi_i, r\right) f\left(\psi_i\right) f\left(r\,|\psi_i\right) dr d\psi_i,$$

where, *i* is an index that represents source type (for example, earthquake, debris flow, mud flow, volcanic flank failure) *r* is the distance from the source to a shoreline location,

$$\nu_i$$

is the mean rate for each source, and

$$\psi_i$$

represents the primary source parameter or set of source parameters (Ward, 2001) for that source. The mean rate is then multiplied by a double integral that contains three probability functions. The function

$$f\left(\psi_i\right)$$

is the probability density function (pdf) for the source parameter. For example, the primary source parameter for earthquakes is seismic moment and, therefore, this pdf would be a modified power-law distribution. The function

$$f\left(r\,|\psi_i\right)$$

is the pdf of the distance for given source parameters and

$$P\left(R > R_0 | \psi_i, r\right)$$

is the cumulative conditional probability that runup at a coastal location will be exceeded for a given distance and given source parameters. This expression is calculated using tsunami generation and propagation models.

Probabilistic Tsunami Hazard Analysis Equation (Discrete Source Zones)

Because numerical propagation models are substituted for ground-motion attenuation relationships in PTHA, and because tsunami propagation paths often are complex, it may not be practical to define the distance pdf in the above equation. Instead, a discrete-source zonation scheme, like the Flinn-Enghdahl zones for earthquakes (Flinn and others, 1974), can be used in place of the $f(r|\psi_i)$ term.

The discrete source zone form of the PTHA equation is given by

$$\lambda\left(R > R_0\right) = \sum_{\mathrm{type}=i} \sum_{\mathrm{zone}=j} \nu_{\mathrm{ij}} \int P\left(R > R_0 | \psi_{\mathrm{ij}}\right) f\left(\psi_i\right) d\psi_i \,,$$

where j is the zone index and i is an index that represents source type. The continuous distance variable (r) has been replaced by discrete source zones. Variation in the source location within a zone is included in the term

$$P\left(R > R_0 | \psi_{\mathrm{ij}}\right).$$

Uncertainties

Given the current lack of data on submarine landslides, there are large uncertainties for each of the components of PTHA. The largest uncertainty is most likely related to the long-term mean rate ν_{ij} of mass failure occurrence in any given region. Although recent research has identified which parameters of mass failures are important for tsunami generation (for example, slide volume, thickness, duration), there is considerable uncertainty in defining the pdf for each of these parameters [that is, $f(\psi_{ij})$]. The complex effect of landslide dynamics on tsunami generation is discussed in the next section.

State-of-the-art numerical modeling of tsunami waves can be used to calculate runup associated with particular submarine landslide parameters [that is, $P(R>R_0)|\ \psi_{ij})$]. Calculating this probability function, however, requires many runs for each source configuration of volume, duration, thickness, and such, thus requiring substantial computational resources. This may be the most tractable part of PTHA where submarine landslides are considered.

Landslide Dynamics

Generation of tsunamis by submarine landslides is a complex process that occurs through distinct temporal phases: failure, post-failure dynamics (for example, debris flows), and turbulent boundary-layer flow (turbidity currents). Because earthquakes trigger most tsunamigenic landslides, inertial displacements of the uppermost compliant

layer in response to strong-ground motion must be considered. Given that the conditions are met for failure to occur, it is likely that a shear dislocation develops at the base of the landslide and propagates in all directions to form the eventual head scarp (up slope) and initial sliding plane (down slope) (Martel, 2004; Petley and others, 2005). The primary concern for tsunami generation is the dynamics of the failed mass, which is described below. During the latter stages of mass movement failure, turbidity currents most often form. Because this process is characterized by turbulent boundary-layer flow and involves smaller changes in seafloor displacement, it is usually not influential in the tsunami generation process.

Many and diverse types of landslides have been classified according to their physics and subaerial observational evidence. The most well-known classification scheme is that of Varnes (1978). There has been an effort to develop a detailed taxonomy of landslides, particularly of the flow type (Hungr and others, 2001). The basic types of mass movements include slow-moving Earth flows (sometimes termed landslides or slides in a specific connotation of the terms), topples, spreads, falls, and fast-moving flows (Locat and Lee, 2002). Two major concerns for tsunami generation are fast-moving submarine debris avalanches and debris flows. A recent classification of debris flows proposed by Coussot and Meunier (1996) is based on two criteria directly related to the mechanical properties of debris flows: solid/water fraction and material type (cohesive versus granular). This classification is seen as an important foundation for understanding the complex dynamics of debris flows that are governed by non-Newtonian rheologies.

In understanding the physics of debris flows, two approaches developed for subaerial flows have been considered: viscoplastic fluid and mixture (or granular) theory. Viscoplastic fluid models have been used to describe submarine muddy debris flows, whereas mixture theory has been used to describe subaerial granular or two-phase flows. The latter has been incorporated into a coupled model for tsunami generation (Fernández-Nieto and others, 2008). In adapting subaerial landslide dynamic models for the submarine environment, the main effect of having water as the ambient fluid, rather than air, is a reduction in gravitational forcing, owing to buoyancy.

Because most tsunamigenic mass movements along continental slopes involve predominantly fine-grained sediment, the viscoplastic fluid model for muddy debris flows is a central model for tsunami generation. A clay content of only 10 percent or more is needed for debris flows to be adequately modeled by viscoplastic rheology (Coussot and Meunier, 1996; Coussot and others, 1998). The longitudinal momentum equation for laminar flow is given by

$$\rho_m\left(\frac{\partial u_x}{\partial t}+u_x\frac{\partial u_x}{\partial x}+u_z\frac{\partial u_x}{\partial z}\right)=\rho_m g\sin\theta-\frac{\partial p}{\partial x}+\frac{\partial \tau}{\partial z},$$

where u_x is the velocity component in the x (down slope) direction, ρ_m is the density of the mud flow, p is the pressure (assumed to be hydrostatic), θ is the slope angle, and τ is the shear stress in the mud flow (Jiang and Leblond, 1993; Imran and others, 2001). The continuity equation for this system is

$$\frac{\partial u_x}{\partial x}+\frac{\partial u_z}{\partial z}=0 .$$

Various nonlinear constitutive relations have been used to relate shear strain rate to shear stress for muddy debris flows (Coussot, 1997), including Bingham plastic, Herschel-Bulkley, and bilinear rheologies. The Bingham plastic fluid is characterized by a finite yield stress (τ_y) such that

$$\mu\gamma=\begin{cases} 0 & \text{if } |\tau|<\tau_y \\ \tau-\tau_y \mathrm{sgn}(\gamma) & \text{if } |\tau|\geq\tau_y \end{cases},$$

where μ is dynamic viscosity and γ is the strain rate . The Herschel-Bulkley rheology is a power-law rheology (i.e., non-Newtonian):

$$K\gamma^n=\begin{cases} 0 & \text{if } |\tau|<\tau_y \\ \tau-\tau_y \mathrm{sgn}(\gamma) & \text{if } |\tau|\geq\tau_y \end{cases},$$

where n and K are material-specific constants. When n=1, the Herschel-Bulkley rheology is equivalent to the Bingham-plastic rheology. The bilinear rheology (e.g., Locat and others, 2004) involves two viscous regimes of flow described by dynamic viscosities at low and high strain rates (μ_l and μ_h, respectively where $\mu_h < \mu_l$):

$$\tau=\left[\tau_{y\alpha}+\mu_h|\gamma|-\frac{\tau_{y\alpha}\gamma_0}{|\gamma|+\gamma_0}\right]\mathrm{sgn}(\gamma),$$

where τ_{ya} is the apparent yield stress relative to the high strain-rate regime and γ_0 is the reference strain rate given by

$$\gamma_0=\frac{\tau_{y\alpha}}{\mu_l-\mu_h} .$$

For these nonlinear rheologies, the no-slip boundary condition along the base of the debris flow results in two flow zones: a shear zone at the base of the flow, where the shear stress is greater than the yield stress, and a plug zone above where the yield stress is not exceeded. The boundary between the two zones is termed the yield interface. In formulating a solution to the momentum equations, the horizontal and vertical velocities and the horizontal velocity gradient are constrained to be continuous across the yield interface (Jiang and Leblond, 1993).

To model granular mass movements that have a smaller proportion of fine sediment and water, the mixture theory that was developed for subaerial debris avalanches (Iverson and Denlinger, 2001) has been adapted in a few cases for the

submarine environment (Fernández-Nieto and others, 2008). For a two-phase solid/fluid mixture in which the fluid velocities and accelerations differ negligibly from the solids, the momentum equation is

$$\rho_m\left(\frac{\partial \mathbf{v_s}}{\partial t}+\mathbf{v_s}\bullet\nabla\mathbf{v_s}\right)=\rho_m\mathbf{g}-\nabla\bullet\left(\mathbf{T_s}+\mathbf{T_f}\right),$$

where $\mathbf{v_s}$ is the solid velocity, T_s and T_f are the stress tensors for the solid and fluid phases, respectively, and the density of the mass movement is calculated from the volume fractions (V_s and V_f) of each phase. The constitutive theory used is intergranular Coulomb friction, modified by pore pressure and Newtonian viscous fluid stresses. For high enough pore pressures, internal friction is reduced greatly, and the mass behaves viscously. It has been argued that mixture theory has limited application in the submarine environment because pore pressure diffusion is likely to be minimal and because a finite yield strength is needed to explain the thickness and mid-slope termination of many submarine debris avalanches (Coussot and Meunier, 1996; Elverhøi and others, 2005); however, mixture theory may be applicable in specific geologic environments, such as carbonate and volcanic-dominated islands, away from continental sources of clay.

Probabilistic Approaches for Determining Landslide Rates

Empirical Approaches

The direct or empirical method of determining submarine landslide probability relies on the dates of events identified in the geologic record. The method is derived from approaches used to determine earthquake probability from datable paleoseismic horizons. The methods described below yield probability and uncertainty estimates, most following an empirical Bayes' method under a variety of assumptions. Bayes' rule is given by

$$\pi(\theta|z) = \frac{L(z|\theta)\pi(\theta)}{\int L(z|\theta)\pi(\theta)d\theta}$$

where θ is the probability parameter of interest and z is the data. On the right-hand side of the equation, the numerator is the likelihood function L times the prior distribution, whereas the denominator is a normalization factor called the marginal probability. The left-hand side of the equation is the posterior distribution.

Binomial-Beta Conjugate Prior

Assuming that the probability (p) of an earthquake on a particular fault or a landslide in a particular region is the same through time, then the problem of estimating p is that of estimating the probability of success in a Bernoulli trial, given a sample of outcomes of previous trials (Savage, 1994). The probability of m successes in n trials is then given by the binomial distribution

$$P(p|m,n) = \left(\begin{array}{c} n \\ m \end{array} \right) p^m (1-p)^{n-m}.$$

The empirical Bayes approach is simplified greatly if a prior probability distribution that is "conjugate" to the likelihood function is chosen: that is, if the resulting posterior distribution is in the same distribution family (e.g., the exponential distribution family) as the prior distribution. The distribution pairs are called conjugate priors. The conjugate prior to the binomial distribution is a beta distribution. To simplify further, parameters of the beta distribution can be chosen to yield a uniform prior distribution (also known as the non-informative prior) with resulting mean and variance given by

$$\langle p \rangle = \frac{m+1}{n+2}$$

$$\sigma^2 = \frac{(m+1)(n-m+1)}{[(n+2)^2(n+3)]}.$$

Example

If there is a geologic record of landslides occurring with inter-event times of 12.25, 20.08, 21.02, 24.07, and 32.05 kyr., then the probability that the next landslide will occur within 26.5 kyr. of the last landslide is given by

$$P(p|4,5) = 30p^4(1-p),$$

with a mean probability of 0.71 and a 95 percent confidence interval ranging from 0.41 to 0.98.

Poisson-Gamma Conjugate Prior

Landslides could be assumed to follow a stationary Poisson process in which the occurrence of landslides is independent from one another (specifically, the number of occurrences in disjoint intervals are independent). This is a more restrictive assumption than for the Binomial-Beta method described above, but it yields more information. The conjugate prior to the Poisson distribution is the gamma distribution with scale parameter beta and shape parameter gamma. The resulting posterior distribution is given by

$$\pi(\lambda|z) = \frac{(\beta')^{\gamma'} \lambda^{\gamma'-1} e^{-\beta'\lambda}}{\Gamma(\gamma')}.$$

The hyperparameters are given by

$$\gamma' = N + (\mu/\sigma)^2$$
$$\beta' = T + \mu/\sigma^2$$

where N is the number of landslides in observation period T (e.g., defined by a datable basal seismic horizon) and μ and σ^2 represent the mean and variance of the rate parameter determined from the data (Mortgat and Shah, 1979; Campbell, 1982).

Example 1

In the Santa Barbara channel there are three landslides of unknown age identified on a seismic-reflection profile and above a horizon with a well-defined date of 170 ka (Fisher and others, 2005).

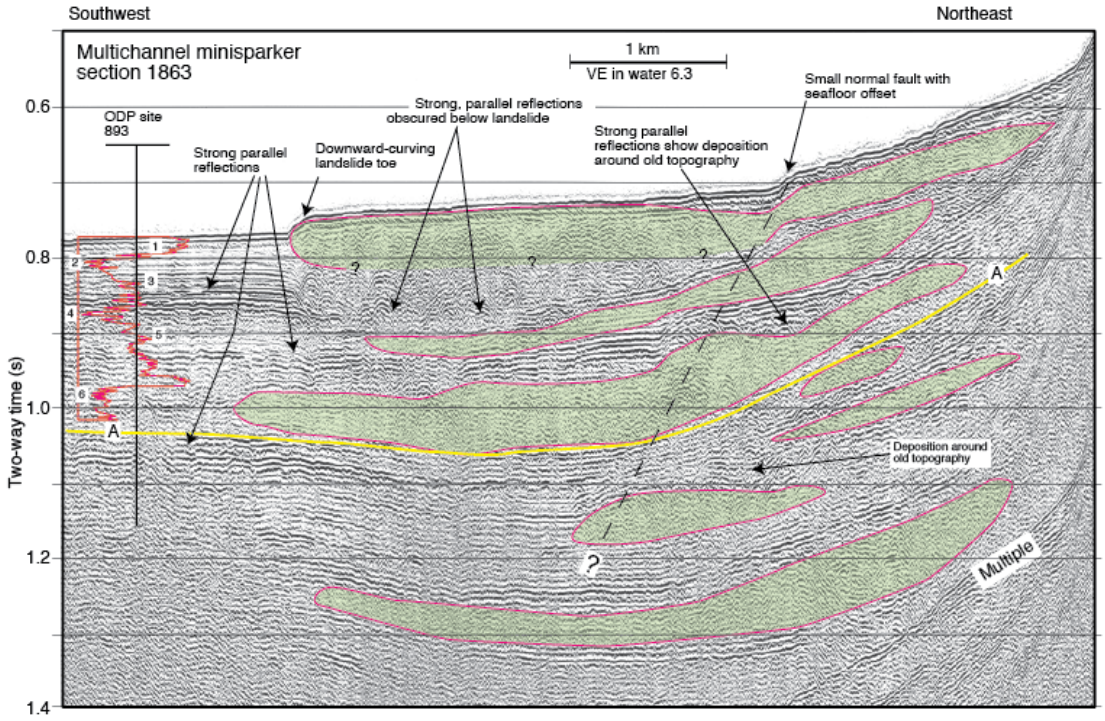

The resulting distribution of possible mean return times ($1/\lambda$) is shown below.

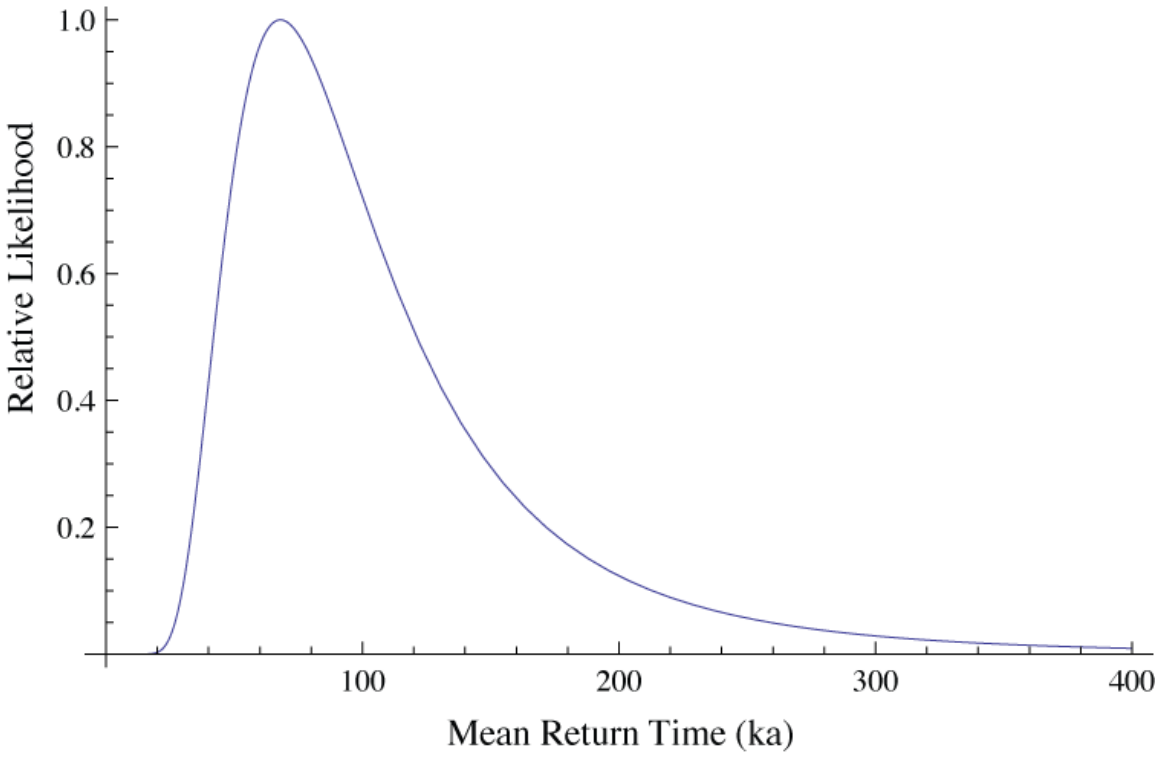

The most likely mean return time is 68 ka, but the 95 percent confidence interval ranges between 29 and 154 ka (Geist and Parsons, 2010).

Example 2

In Port Valdez, 6 debris flows were imaged in seismic reflection data, all presumed to by younger the 6 ka (Ryan and others, 2010). The resulting distribution of possible mean return times ($1/\lambda$) is shown below:

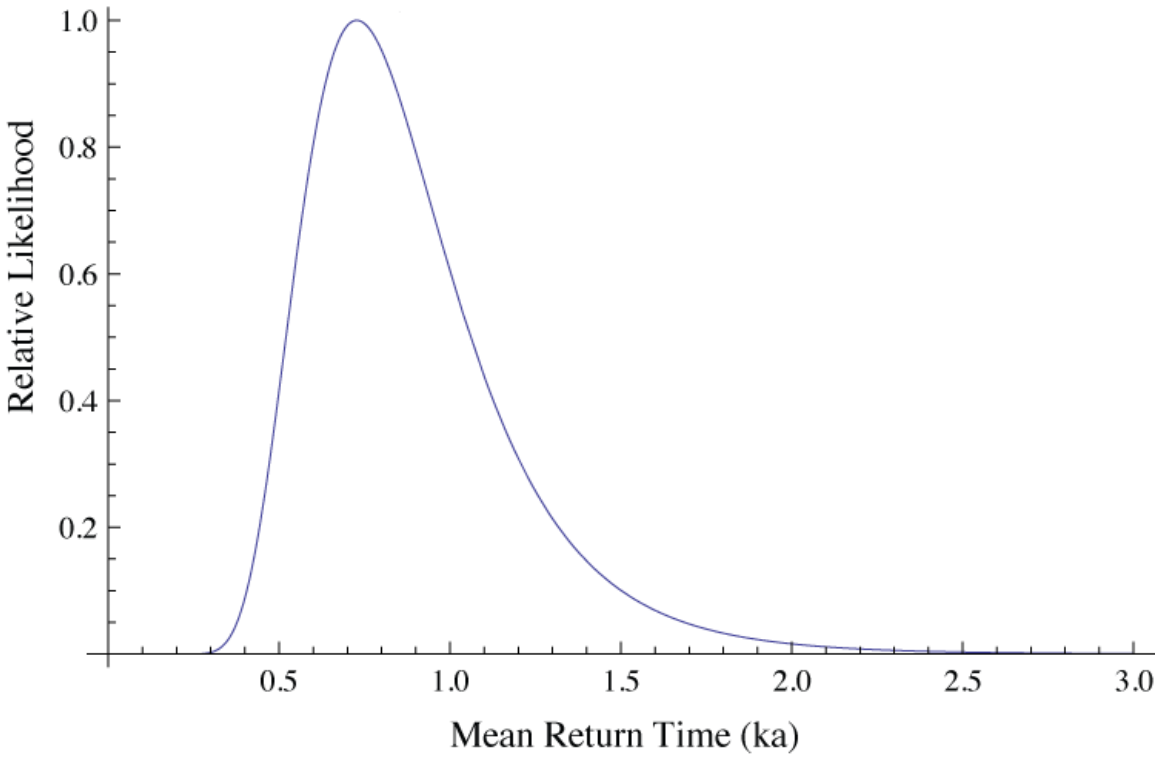

The most likely mean return time is 730 years with a 95 percent confidence interval ranging between 410 and 1,300 years (Geist and Parsons, 2010). The rate of landslide occurrence in Port Valdez is significantly higher than offshore Santa Barbara.

Monte Carlo Method

The Monte Carlo and Baysian inference methods described below are developed for a situation in which probability is estimated from a small number of events, each of which has been dated with some uncertainty. For example, a drill hole penetrates several landslide events for which there are dates for the strata above and below, bracketing the age when a given landslide occurred (e.g., Normark and others, 2004). The conjugate prior methods described above are primarily for the situation in which there is only a datable horizon below a sequence of landslides.

The Monte Carlo method developed by Parsons (2008) relies on sampling a given distribution a large number of times to determine the most likely distribution parameters that fit the observed range of dates available for each event and the range of uncertainty in the distribution parameters. Unlike other empirical methods, the Monte Carlo method is not derived directly from Bayes' rule.

Example

Several paleoseismic horizons have been dated in southwest Washington representing large earthquakes along the Cascadia subduction zone (Atwater and others,

2004). The Monte Carlo method is used to estimate the two parameters for a Brownian Passage Time (BPT) distribution for earthquake occurrence (Matthews and others, 2002). The distribution parameters of the BPT distribution are the mean inter-event time and apreriodicity (or coefficient of variation).

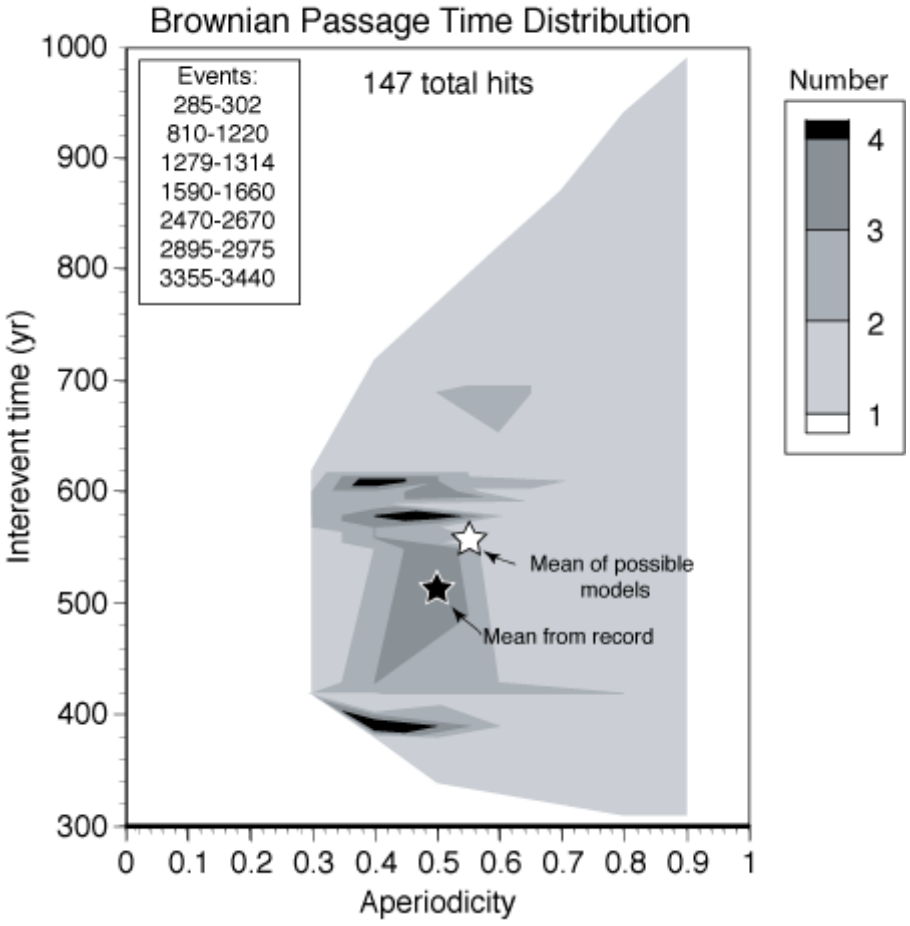

For increments of each distribution parameter, a sequence of seven random samples is drawn from the associated probability distribution to see if each sample falls within the age range for each event. If no samples lie between events or in the open intervals before the first event and after the last event, then one "hit" is recorded for that set of distribution parameters. This is repeated millions of times for each set of distribution parameters, and the total number of hits is tallied, yielding the contour plot displayed above. The results yield mean, median, and modes of the most likely distribution parameters and a range of uncertainty. In the figure above, "mean from the record" is the mean interevent time using the center age of each event.

Bayesian Inference Method

Similar to the Monte Carlo method, the Bayesian Inference Method was developed by Ogata (1999) to determine the best fit distribution parameters given a

sequence of geologic events with uncertain ages. In this case, Bayes Rule is used in the opposite sense, where the most likely occurrence times are estimated by way of the posterior conditional probability distribution:

$$\pi\left(t_1, \ldots, t_n \middle| \theta\right) = \frac{L(\theta; t_1, \ldots, t_n) \prod_{i=1}^{n} \pi_i(t_i)}{\mathcal{L}(\theta)},$$

where

$$L\left(\theta; t_1, \ldots, t_n\right)$$

is the likelihood function. The semicolon separates the fixed parameter(s) of the inter-event distribution model (theta) and the data (estimated times of occurrence).

$$\pi_i\left(t_i\right)$$

are the probability densities for the landslides occurring within a particular age range. Several different prior distributions were tested by Ogata (1999), including the Dirac delta function (centered data), a uniform distribution, and a triangular distribution.

$$\mathcal{L}(\theta) = \int \ldots \int L\left(\theta; t_1, \ldots, t_n\right) \prod_{i=1}^{n} \pi_i\left(t_i\right) dt_1 \ldots dt_n$$

is the integrated likelihood of the parameter θ.

The integrated likelihood is key to the Bayesian Inference Method in estimating the parameters of the inter-event distribution model and in evaluating competing models. The model parameters are determined by maximizing the integrated likelihood function with respect to theta. In the case that the occurrence times are known exactly, the integrated likelihood reduces to the ordinary likelihood function. Because there is uncertainty in each of the dated landslides, however, the multiple integration expressed in the above equation needs to be computed, most often using numerical methods. Once theta is estimated, then the most likely occurrence time for each landslide can be determined through the posterior distribution. In addition, once the likelihood is known, then the goodness of fit for the distribution model and priors can be evaluated using the Akaike Information Criterion (AIC).

Example

The example below is from Ogata (1999), in which he uses the Bayesian Inference Method on 11 earthquake dates along the West Nagano Basin fault. Two of the dates are exact (historical earthquakes), whereas the rest are geologic dates with associated uncertainties. The table below lists the results of the Bayesian Inference Method using different inter-event distribution models (exponential, lognormal, etc.) and three different prior distributions. By using the AIC, a decision can be made as to which model and which model parameters best fit the data. (See the comment below the table for an explanation of superscripts in the AIC column.) MRT is the mean return time associated with each case.

Table 8. West Nagano Basin Fault Events

Interval Density	AIC or ABIC	Real scale		Normalized		MRT
		Parameter 1	Parameter 2	Parameter 1	Parameter 2	
Exponential	144.7	9.8×10^{-4}	–	1.0	–	1016.
		Centered Data (Dirac's Delta Prior)				
Lognormal	129.8	7.0	0.25	0.037	0.25	1087.
	127.4[a]	(6.9)	(0.2)	(–0.025)	(0.2)	1011.
Gamma	129.0	0.015	16.	15.	16.	1087.
	127.8	(0.025)	(25.)	(25.)	(25.)	1016.
Weibull	130.7	6.1×10^{-14}	4.3	0.50	4.3	1087.
	129.1	1.9×10^{-12}	3.8	0.68	3.8	–
Doubly Exponential	131.9	3.8×10^{-5}	0.0037	0.039	3.7	1101.
	129.9	(3.9×10^{-5})	0.0036	(0.04)	3.7	1099.
		Uniform Prior Distribution				
Lognormal	135.7	7.0	0.20	0.047	0.20	1087.
	132.7	(6.9)	(0.2)	(–0.025)	(0.2)	1011.
Gamma	135.7	0.022	24.	22.	24.	1087.
	132.6[b]	(0.025)	(25.)	(25.)	(25.)	1016.
Weibull	135.5	4.7×10^{-18}	5.6	0.43	5.6	1089.
	133.6	1.1×10^{-20}	(6.5)	0.38	(6.5)	1098.
Doubly Exponential	135.4	8.9×10^{-6}	0.0053	0.0091	5.4	1091
	133.5	1.4×10^{-5}	(0.0049)	0.014	(5.)	1084.
		Triangular Prior Distribution				
Lognormal	132.8	7.0	0.21	0.0046	0.21	1088.
	129.8	(6.9)	(0.2)	(–0.025)	(0.2)	1011.
Gamma	132.7	0.021	23.	21.	23.	1088.
	129.6[b]	(0.025)	(25.)	(25.)	(25.)	1016.
Weibull	132.4	2.1×10^{-18}	5.8	0.42	5.8	1090.
	130.5	1.1×10^{-20}	(6.5)	0.38	(6.5)	1100.
Doubly Exponential	132.4	7.9×10^{-6}	0.0055	0.080	5.6	1091.
	130.5	1.4×10^{-5}	(0.0049)	0.014	(5.)	1079.

The first row for each model distribution is for unrestricted parameters and the second row is for smallest AIC or ABIC among the restricted parameters; parentheses indicate fixed values (see text for further explanation). [a] Overall best fitted value for the data set. [b] Best fitted value for each distribution.

Geotechnical Approach: From Earthquake to Landslide

The temporal development of slope failure is fundamental to understanding the landslide process and also is important to the assessment of landslide-generated tsunami, whose runup depends to a large extent on the size of the landslide (for example, Geist and others, 2009a). Several studies have identified retrogressive failures (for example, Harbitz, 1992; Locat and others, 2009), but it is unclear whether these failures occurred during the same event or were separate in time. In the absence of direct observations, scientists have made assumptions about failure dynamics. The most common assumption is that a landslide process is a cascade or an avalanche process (Densmore and others, 1998; Guzzetti and others, 2002; Malamud and Turcotte, 2006) known as self-organized criticality (Bak and others, 1988; Hergarten, 2003). The cascade process assumes that failure nucleates in one or more locations, spreads to surrounding regions, and can coalesce to generate large failures. This process often is simulated by cellular-automata models (e.g., Malamud and Turcotte, 2006). The area-frequency distribution of the cascade process is an inverse power law (e.g., Guzzetti and others, 2002). By its nature, it is an additive process whose duration can vary widely and cannot be determined at the

start of the process (Turcotte and Malamud, 2004). The most famous example of an additive process in the Earth sciences is the frequency-magnitude relationship of earthquakes (Gutenberg and Richter, 1944):

$$\log N = a - bM$$

where N is the number of earthquakes with magnitude greater than M occurring during a given time, and a and b are constants. This distribution implies that earthquakes grow from nucleation points and their final magnitude cannot be predicted (Stein and Wysession, 2003, p. 274).

An inverse power law distribution also was invoked for different physical aspects of subaerial (Sugai and others, 1994; Dai and Lee, 2001; Guzzetti and others, 2002; Dussauge and others, 2003; Malamud and others, 2004) and submarine (ten Brink and others, 2006a; Micallef and others, 2008) landslides. In the majority of these publications, however, the inverse power law distribution applies only to a truncated portion of the dataset (Stark and Hovius, 2001). To fit the entire range of landslide areas, Malamud and others (2004) proposed a three-parameter inverse Gamma distribution and Stark and Hovius (2001) proposed a double Pareto function. The misfit of an inverse power law distribution to the portion covering the smallest sizes was attributed to undersampling (Burroughs and Tebbens, 2001; ten Brink and others, 2006a), to an artifact of the mapping resolution (Stark and Hovius, 2001), or to the transition from a friction-controlled resistance to a cohesion-controlled resistance (Guzzetti and others, 2002).

A few landslide datasets, however, have distributions that are not easily approximated by an inverse power law distribution. Issler and others (2005) obtained a logarithmic distribution for the volume of depositional lobes from the Storegga slide. Lognormal distributions were found for the areas of landslides in Kashmir (Dunning and others, 2007) and for volumes of deposits of prehistoric turbidity currents in Italy (Talling and others, 2007). Chaytor and others (2009) obtained a lognormal fit to the size distribution of the areas and volumes of 106 submarine slope failure along the Atlantic continental slope (R^2=0.9938) (Figures 1 and 2). Many of the landslides, especially open-slope landslides, initiate on these low-angle slopes (<2 degrees) (Twichell and others, 2009). The slope of the continental margin could be further characterized as monotonic: the direction of greatest slope is oriented in the same general direction (seaward) over a large area (fig. 1).

Hypothesis

A simple earthquake-triggered landslide mechanism can produce area distributions that can be approximated by a lognormal distribution. Although an inverse power law can sometimes approximate the tails of these distributions, the physical significance of an inverse power law distribution for landslides is questionable. For example, it may be incorrect to assume that during an event the failure always grows from single or several point-failures and that its final size is unpredictable. (Circumstances where the final landslide size may be unpredictable cannot be discarded. One such mechanism is discussed with respect to Puerto Rico.) The failed material may coalesce into debris flows and turbidity flows as it moves downslope (Tripsanas and others, 2008), but the downslope movement itself does not excavate significant amounts of new material.

Although it is difficult to assess the general validity of this hypothesis, at least one historical record suggests that it could be correct in some cases. Multibeam bathymetry and side-scan sonar surveys of the 1929 Grand Banks landslide, which was triggered by a M7.2±0.3 earthquake, did not reveal evidence for a single major headwall scarp, or for a massive slump region (Piper and others, 1999; Mosher and Piper, 2007; D. Mosher, written comm., 2007). Two-thirds of the total failure area were characterized by patchy failures, with intervening areas showing no evidence of failure. Had the failure been a downslope or upslope cascading process from one or several nucleation points, it is likely that the entire area would have shown evidence of seafloor failure. The seismological record also is compatible with the hypothesis that failure occurs simultaneously in the area affected by shaking. If landslides nucleate in one location and then propagate along the failure plane similar to earthquake propagation, we would expect large double-couple landslide earthquakes to occur when a large submarine slope failure takes place; however, such earthquakes were not detected during the 1929 Grand Banks (Bent, 1995) or the 1998 Papua New Guinea tsunamigenic landslides (Okal and Synolakis, 2001).

Simulations of Earthquake-Induced Landslides

To test the viability of the hypothesis, Monte Carlo simulations of earthquakes and their expected failure areas were generated and their area distribution was compared with the observed distribution along the U.S. Atlantic continental margin (figs. 1 and 2). The maximum expected failure area was estimated using a slope stability analysis with undrained strength properties following the method and parameters outlined by ten Brink and others (2009c). The method is reviewed here briefly.

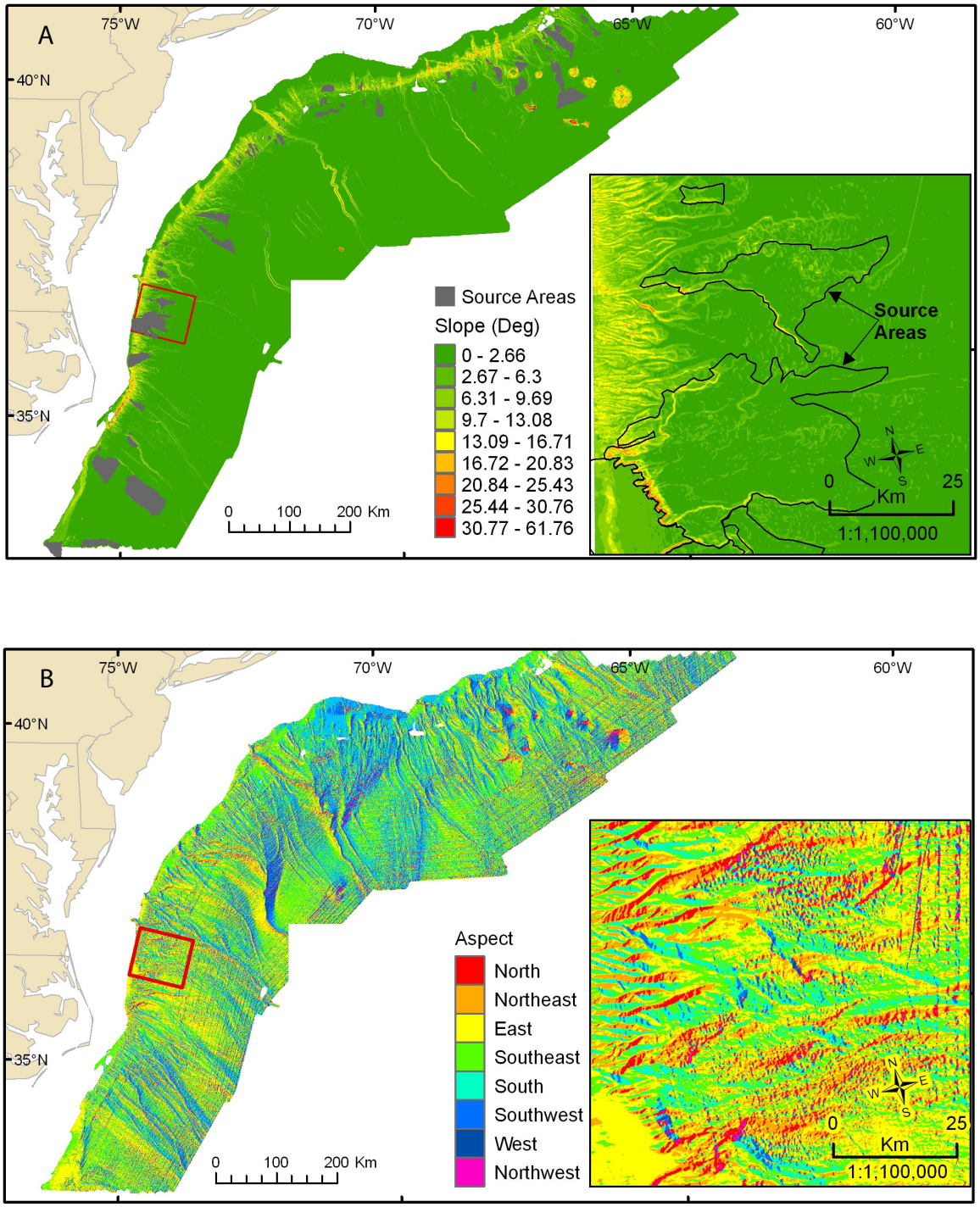

Figure 1. A, Slope gradient of the U.S. Atlantic margin; B, Slope direction (known as aspect) of the Atlantic margin.

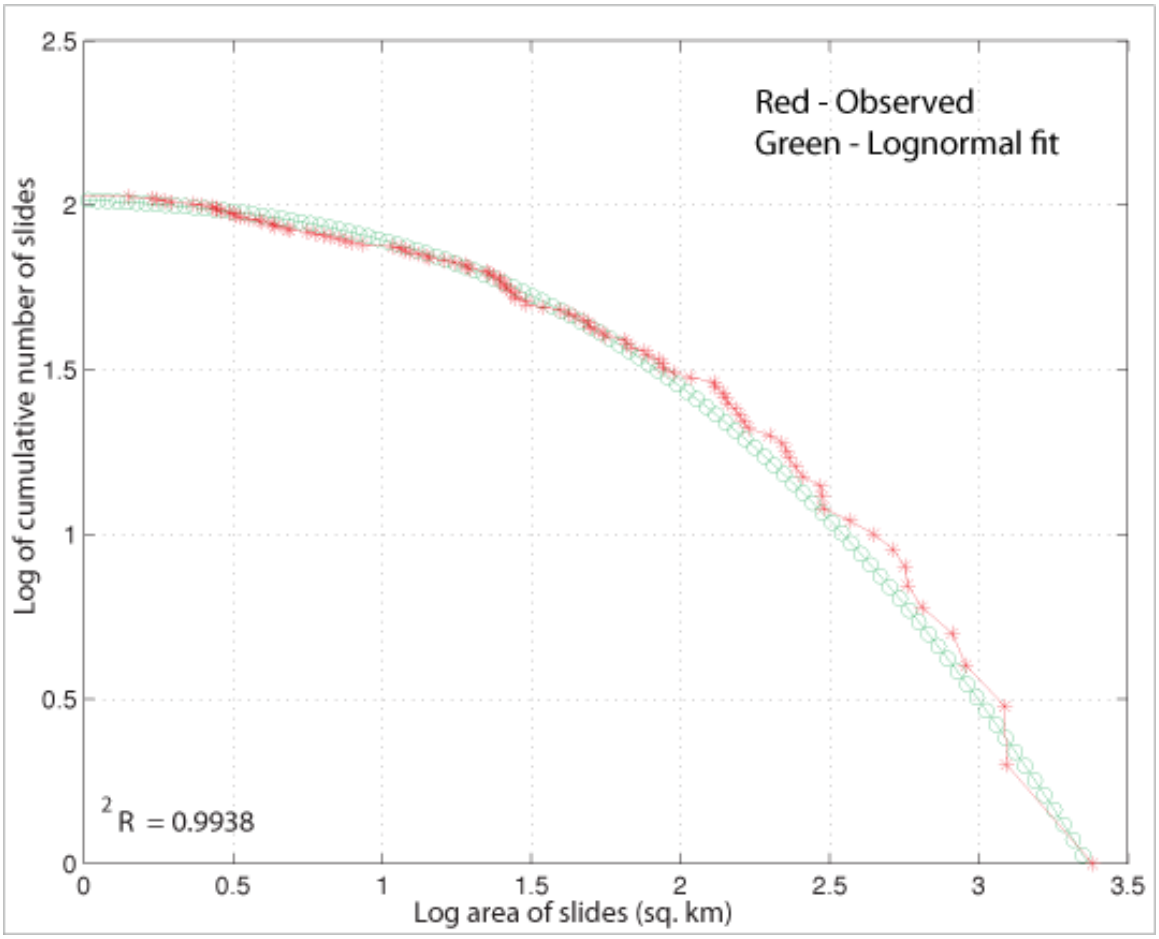

Figure 2. Cumulative distribution of landslide areas along the Atlantic margin and their fit by lognormal function.

Slope failure of sediments is assumed to initiate when the combined static downslope gravitational stress plus the dynamic earthquake loading, exceeds the undrained shear strength. For enough cycles, this induces permanent strain in the slope. The vertical ground-motion component contains little of the total energy of shaking and, therefore, is ignored in strong-motion studies (Harp and Wilson, 1995). The critical pseudo-static stress (a simplified representation of the dynamic loads) depends on the slope, sediment density, and the ratio of shear strength to vertical load; however, to cause significant displacement of the material, sediment shear strength, (k_y), must be ≤ 15% of the peak earthquake acceleration (k_{PSA}) (Hynes-Griffin and Franklin, 1984; Lee and others, 2000). The peak earthquake acceleration as a function of distance from the rupturing fault ($k_{PSA(r)}$) used here is based on empirical and hybrid-empirical attenuation relationships derived from accelerograms and adjusted for the eastern U.S. (Campbell, 2003). The attenuation relations assume hard rock with shear-wave velocity of 2,800 m/s. A site amplification of 3.5 is used (Boore and Joyner, 1997) to account for the measured shear-wave velocity of 300 m/s of shallow sediments on the Atlantic continental slope. A peak spectral acceleration at a period of 0.75 s was chosen because the thickness of the sliding layer is typically 20-100 m. More details about the choice of these and other parameters are provided by ten Brink and others (2009c). The maximum failure distance

from a rupturing fault (r_{max}), therefore, is the distance at which the modified earthquake acceleration is equal to the sediment shear strength,

$$3.5 \times 0.15 \times k_{PSA} = k_y.$$

The maximum slope failure area, A_L, can be calculated by using the maximum distance to failure, r_{max}. The maximum failure area is, to a first approximation, a rectangle containing the fault trace, whose length is the fault length L and whose half-width is r_{max}, plus two half circles with radii of r_{max} at either end of the fault as given by

$$A_L = p\, r_{max}^2 + L \times 2\, r_{max}.$$

Fault rupture length (L) as a function of earthquake magnitude (M) is based on the empirical relationship of Wells and Coppersmith (1994) for all faults,

$$L = -2.44 + 0.59\, M$$

The calculated area as a function of magnitude is a maximum failure area and assumes uniform energy release along the fault. To further simplify the simulations, a generic depth profile is assumed (fig. 3), which is averaged qualitatively from 6 depth profiles of the U.S. Atlantic continental margin (fig. 1) and which represents a several thousand kilometer sector of the margin. The ruptured faults are assumed to be parallel to the shelf edge to reduce the simulations to 2D. Deviations of fault orientation from this idealized orientation will be accounted for later.

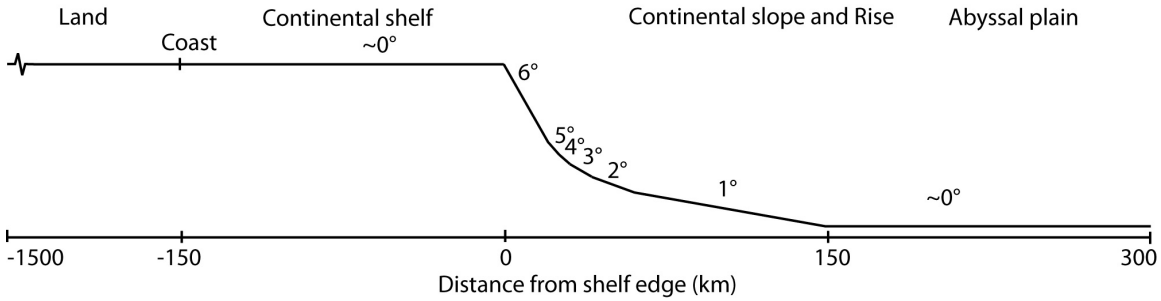

Figure 3. Simplified view of the continental margin that was used for Monte Carlo simulations.

The Gutenberg-Richter (G-R) frequency magnitude distribution ($\log N = a - bM$) was used to generate the earthquake distribution. The G-R distribution is valid for sufficiently long time intervals and large areas. Observed slope failures along the U.S. Atlantic continental margin and in many passive margins have likely happened over a period of several tens of thousands of years (Lee, 2009). For the U.S. Atlantic continental margin, it was assumed that the U.S. east coast, from 1,300 km inland of the shelf edge to 500 km seaward of the shelf edge, is a sufficiently large area to follow the G-R earthquake distribution. In the model, the 150-km-wide continental slope begins 150 km seaward of the coast, which mimics the geometry of the U.S. Atlantic continental margin.

Earthquakes with magnitudes between 4.5 and 7.5 were placed at random locations across this area. The number of earthquakes in each magnitude follows the G-R magnitude distribution. A total of 2,348 earthquakes were placed at magnitude intervals of 0.2 to 0.3, assuming that for every one M7.5 earthquake, there are 10 M6.5 earthquakes, 100 M5.5 earthquakes, and so on. Magnitudes greater than 7.5 were not considered because the maximum earthquake magnitude on the U.S. east coast is assessed to be M7.5 (Frankel and others, 1996; Mazzotti and Adams, 2005). For

earthquakes with magnitudes <4.5, the slope stability analysis does not predict the generation of landslides in slopes ≤6 degrees. This prediction is in agreement with observations of earthquake-induced subaerial landslides in the U.S., which show that earthquakes with local magnitude M_L<4 do not generate landslides, and with inferences suggesting that rock slumps, block slides, rapid soil flows and subaqueous landslides are not generated by earthquakes with magnitude M_L<5 (Keefer, 1984).

It could be argued that the dissected upper continental slope can give rise to many more small landslides than is considered with this model of a generic slope. An examination of slope dip offshore of Chesapeake Bay shows that slope dissection by canyons whose walls exceed 6 degree slope is generally limited to a ~10-km-wide strip of the slope (inset in fig. 1). The probability of any of the 1,000 M4.5 earthquakes occurring in this 10 km-wide-strip of the 1,500 km-wide-zone of simulation is 1,000*10/1,500 km, or 2 earthquakes will be added on average to the simulation results. If M4 earthquakes can generate landslides in slopes that exceed 6°, 4 additional small earthquakes will be added; however, the canyon walls, which are cut into pre-Pleistocene rocks (Pratson and others, 1994), also have a higher strength than was considered in the simulations. The increased wall strength means that the ground-shaking amplification is likely to be smaller than the site amplification factor of 3.5 used in the simulations, and therefore, the peak ground acceleration (k_{PSA}) necessary to cause significant failure should be larger than calculated in these simulations. The area distribution of landslides along the Atlantic continental slope will, therefore, probably not change significantly because small earthquakes cannot generate sufficient ground shaking to cause landslides in these walls.

Results

1. Spatial distribution of earthquakes that could generate landslides

The maximum failure area for each of the earthquakes was calculated using the slope stability analysis (ten Brink and others, 2009b; ten Brink and others, 2009c). Earthquakes that are located within the continental slope generate slope failure; earthquakes that are far away from the continental slope do not generate slope failures. Those earthquakes that are in the vicinity of the landward and seaward edges of the continental slope generate smaller regions of slope failure within the continental slope. For example, an M7.5 earthquake must be within 100 km of the continental slope to cause slope failure (ten Brink and others, 2009c). This earthquake location criterion allows us to define a spatial "danger zone" for earthquake-generated landslides. Earthquakes falling outside this zone are not expected to generate landslides and tsunamis.

2. Landslide size distribution in Atlantic reflects magnitude of ground shaking

The cumulative distribution of the earthquake-induced landslides from 2,348 simulated earthquakes ranging from M4.5 to M7.5 is plotted on a log-log plot (fig. 4*A*). Note that only 80 to 150 landslides are generated per simulation because the majority of the earthquakes are located too far inland to affect the continental slope. Because the location of earthquakes cannot be predicted, the calculation is repeated 1,000 times with 1,000

different random distributions of earthquake locations. The result (fig. 4*B*) shows a consistent cumulative area distribution, with abundant landslides having areas between 10 and 100 km^2, fewer landslides with areas <3 km^2, and few landslides with areas >1,800 km^2 (fig. 4*C*). The 1,000 modeled landslide distributions fit well a lognormal distribution (R^2>0.97). Hence, the paucity of small landslides relative to the number predicted by an inverse power law relationship may not be the result of undersampling, but instead may be caused by the fact that small magnitude earthquakes cannot generate landslides unless the seafloor slope is very steep, whereas the areal extent of seafloor with steep slopes is small. Although some of the realizations show a linear tail of cumulative area distribution, the curve does not have a distinct slope break that would allow a certain range of the population to be fit by an inverse power law curve. Simulations with a limited earthquake magnitude range (M4.5-M6.3) show a good fit to the area distribution of 106 landslides along the Atlantic continental slope (fig. 4*D*). The observed good fit suggests the possibility that the shape of the observed area distribution of submarine landslides may be indicative of the range of earthquake magnitudes in that area. Similar studies in other regions are needed to verify this suggestion.

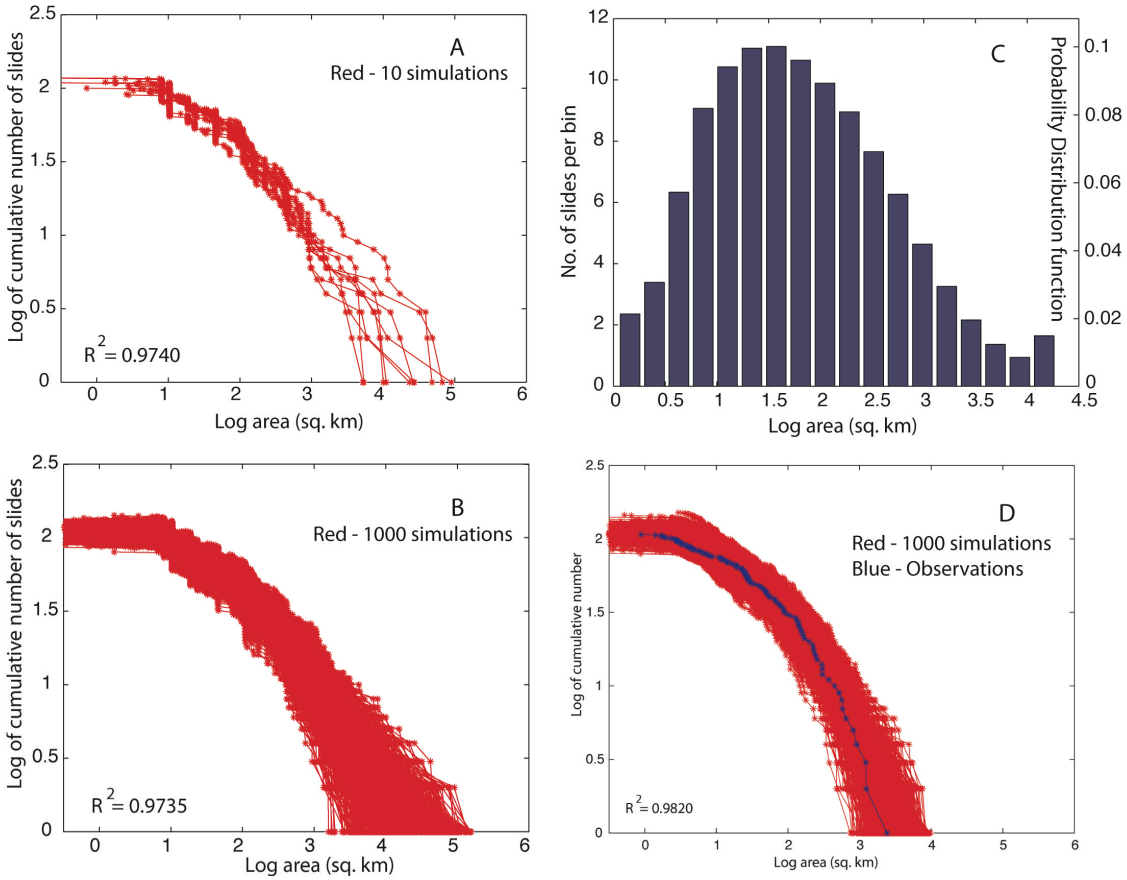

Figure 4. See text for description.

The failure area calculated by the slope-stability analysis is a maximum area. It is likely that the fault does not have a uniform energy release and only part of the area fails during an earthquake, the rheology and pore pressure are not spatially uniform, or the

fault orientation is not parallel to the strike of the margin, as in our simplified simulations. To mimic these situations, the predicted failure area is decreased by multiplying each failure area from each earthquake by a random factor ≤1. In the absence of information about the probability distribution of this random factor, a range of 0.3-1 was assumed, with all values between 0.3 and 1 having an equal probability. The observed landslide distribution along the U.S. Atlantic margin is plotted at the center of the 1,000 simulated curves that were generated with a multiplier range between 0.3 and 1 (fig. 4*D*), whereas it has smaller areas relative to most curves generated by simulations where the maximum area is always expected to fail (multiplier of 1; fig. 5). The comparison to observations therefore, suggests that slope failures generally do not reach their maximum calculated area, as was expected intuitively.

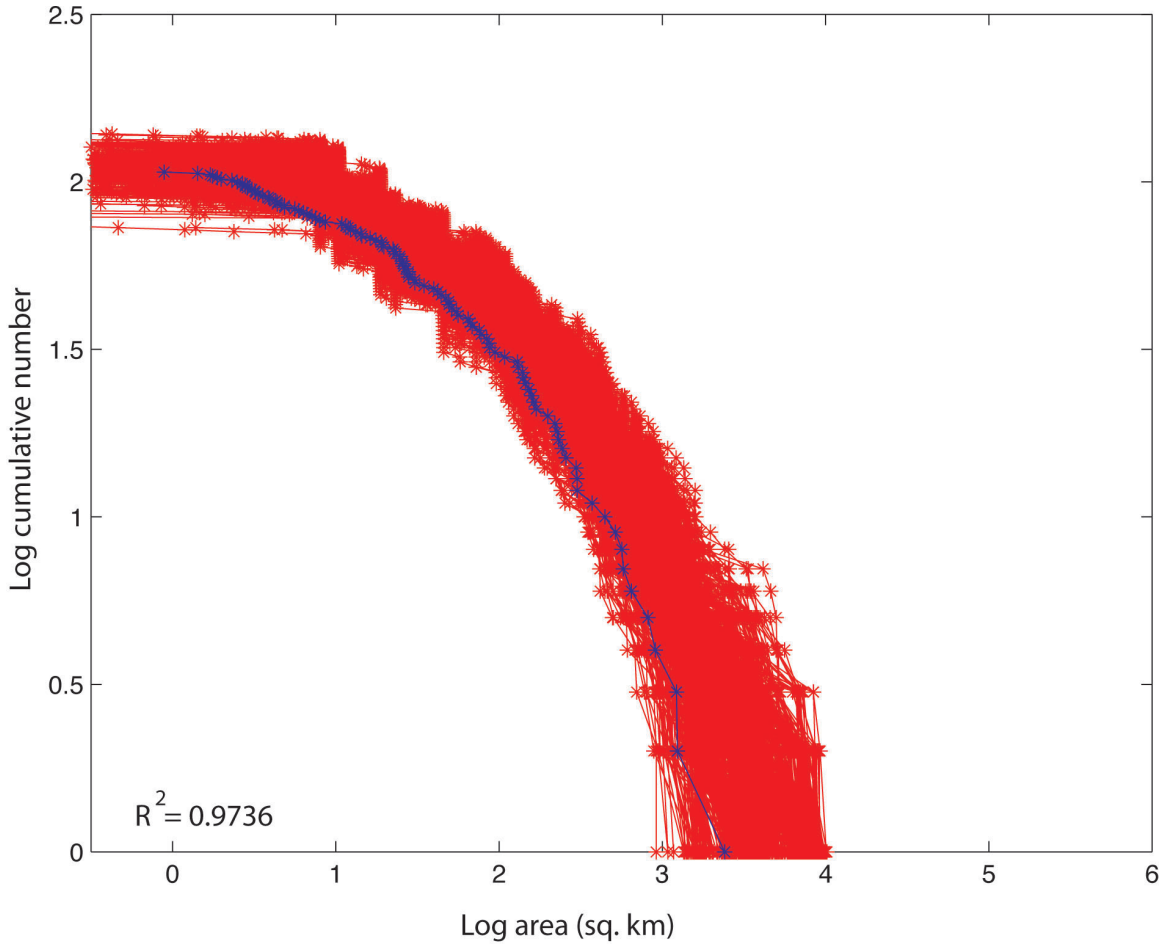

Figure 5. See text for description.

3. Power law distribution of landslides north of Puerto Rico

Translational slides of noncohesive material, such as along the U.S. Atlantic margin, may undergo simultaneous slope failure over a large area during ground shaking; however, other submarine landslides may obey an inverse power law. For example, the inverse power law distribution of areas and volumes of submarine landslides north of Puerto Rico (ten Brink and others, 2006a) may be controlled by the distribution of fractures and not by earthquake magnitude. These mostly rotational landslides erode the edge of a massive, tilted carbonate platform. Fissures and fractures observed in multibeam bathymetry images at the edge of the platform (ten Brink and others, 2006b) probably develop from tensile stresses and grow as a result of carbonate dissolution in a system of seawater circulation. Slope failures during earthquakes may follow these fractures. Tensile fracture systems (Katz and Aharonov, 2006) and faults (Scholz and Cowie, 1990) have been shown to obey an inverse power law distribution in the lab and in the field, attesting to their progressive development.

Summary

The area distribution of submarine landslides along the U.S. Atlantic continental slope and other supporting evidence was used to argue that landslides initiate simultaneously throughout the area affected by ground shaking. The slide products (debris flow, debris avalanche, turbidities) do not entrain significant volumes of new material during the runout. This hypothesis contradicts previous interpretations of landslides as a cascading avalanche, or self-organized critical process, where the landslide nucleates in one or few locations and propagates from there to the entire landslide region. For a given earthquake magnitude, the predicted maximum failure area from slope stability analysis is comparable to the maximum observed area that encompasses all subaerial landslides from a single earthquake-triggered event. The many individual landslides within the observed land area can be perceived in the context of the hypothesis for this study as many independent nucleating points triggered by a single event. The hypothesis presented here, implies that the maximum area of landslides generally is predictable from the characteristics of the triggering event, however, how much of that area will fail depends on local variations in slope angle, material strength, and pore pressure, and the presence of pre-existing fractures.

Challenges

There are a multitude of challenges for incorporating landslides into PTHA, particularly at design probabilities of interest to the NRC. For example, the conventional PTHA formulation assumes independence among source parameters—an assumption that may not be true for landslides.

Incorporation of Tides—Nonlinear Effects

The tidal stage during a tsunami cannot be predicted and is, therefore, a source of aleatory uncertainty in probabilistic calculations. Mofjeld and others (2007) recognized that the tsunami waves occur over a long duration and can span several tidal cycles. In this method, the tidal probabilities are integrated with the tsunami-probability calculations.

Linear Method

Consider the far-field case where only one earthquake scenario (magnitude, slip, area) is considered per source region (*j*). For each tsunami amplitude A_j (corresponding to each *j* source), the tides produce a probability density function *f(y,A)* that describes the distribution in height of the maximum waves, where y is the total wave height including tsunami and tidal amplitudes. To get the exceedance rate for the *j*th source as a function of *y*, the corresponding pdf is integrated as follows:

$$F_j\left(y, A_j\right) \equiv \int_y^{\infty} f\left(y', A\right) dy'$$

To get an explicit form for $F(y,A)$, a Gaussian distribution (Mofjeld and others, 2007) is a reasonable approximation to the pdf:

$$f(y,A) = B\exp\left[-(y-\eta_0)^2/2\sigma^2\right], \quad B^{-1} = \sqrt{2\pi}\sigma$$

where

$$\eta_0(A) = A + \mathrm{MSL} + C(\mathrm{MHHW} - \mathrm{MSL})\exp\left[-\alpha\left(A/\sigma_0\right)^{\beta}\right]$$

$$\sigma(A) = \sigma_0 - C'\sigma_0 \exp\left[-\alpha'\left(A/\sigma_0\right)^{\beta'}\right].$$

The parameters *C*, α, β, C', α', and β' are specific to the tides at a given location (Mofjeld and others, 2004). The integral $F(y,A)$ then becomes

$$F(y,A) = \frac{1}{2}\mathrm{erfc}\left[\left(y-\eta_0\right)/\sqrt{2}\sigma\right], \quad \mathrm{erfc}(z) \equiv 1 - \mathrm{erf}(z),$$

where erf(*z*) is the standard form for the error function.

The rate at which $y' \geq y$ for a given source (λ) is the mean rate of the design earthquake (ν) multiplied by F_j:

$$\lambda_j\left(y' \geq y\right) = \upsilon_j F_j\left(y' \geq y\right).$$

If, for all source regions, there is only one design earthquake per region, then the aggregate exceedance rate would be (since we are dealing with discrete regions):

$$\lambda\left(y' \geq y\right) = \sum_j \lambda_j\left(y' \geq y\right)$$

Effect of Nonlinearity

The preceding methods assumed linear superposition of tide and tsunami waves and are, therefore, treated as being independent. For landslide tsunamis that can be nonlinear, independence between the two phenomena breaks down. In terms of the notation described in the Linear Method above, tsunami amplitude (A) depends on the tidal constants.

The joint probability of tides and tsunamis considering the nonlinear effects can be determined by Monte Carlo methods in which a large number of numerical simulations are done under different tidal conditions. The computational resources required to determine the probability distribution in this way are likely to be substantial

It may be possible to use copulas to determine the joint distribution in place of Monte Carlo methods. Copulas contain all the information of the dependency structure for a multivariate distribution. Sklar's (1959) representation theorems states that a joint cumulative distribution function $H(x,y)$ can be represented by

$$H(x,y) = C\left[F(x), G(y)\right],$$

where $F(x)$ and $G(y)$ are marginal distributions and C is the copula. There are a number of copulas that can be chosen that reflect the dependence structure between $F(x)$ and $G(y)$, rather than the distributions themselves. Examples of the use of copulas can be found in hydrology (Favre and others, 2004; Genest and Favre, 2007) and seismic hazard analysis (Page and Carlson, 2006) and conceivably can be adapted for use in PTHA.

Temporal and Spatial Clustering of Sources

Temporal and spatial clustering beyond what is predicted by a Poisson point process is not accommodated in the basic PTHA Framework. Temporal and spatial clustering in landslides can arise from two causes: seismic triggering of multiple landslides and retrogressive failure. For the former, the temporal scale of clustering is small, approximately on the order of ground-shaking duration, whereas the spatial scale of clustering can encompass a broad region. In contrast, for retrogressive failures, the spatial scale of clustering is limited to the main failure dimensions, whereas the temporal scale can range from hours to days (Masson and others, 2006) or to longer time scales.

During strong shaking from an earthquake, multiple discrete regions can fail. The failure can be distributed over a wide region and occur nearly simultaneously or it can be delayed, depending on material and pore-pressure properties of the sediment. An example of spatial clustering of landslides from seismic triggering is the 1929 Grand Banks landslide (Piper and others, 1999). Lynett and Jimenez (2011) (see also Haugen and others, 2005) have developed a 1HD cross-shore model where, for a given number of

individual slides, parameters such as downslope width and delay of initiation are randomized. Hazard curves can then be compared to that for a single-body landslide to assess the effect of source complexity on probabilistic assessments of wave height.

Temporal and small-scale spatial clustering can occur from retrogressive failure following a large landslide or other localized geological conditions that preferentially result in failure. Modeling studies have indicated that retrogressive failure occurs after the main failure in the presence of shear softening (Masson and others, 2006). Retrogressive failures appear to occur most frequently on low-slope continental margins, although volcanic flank failures, such as in the Canary Islands, also appear to be retrogressive. Perhaps the best analyzed retrogressive failure is the Storegga landslide, which appears to have been initiated at the lower slope of the Norwegian margin (Haflidason and others, 2004).

There are few analogs in PSHA that could be used to formulate a PTHA model that involves clustered sources. The incorporation of spatial and temporal cluster into PSHA methodology has been attempted only recently, owing to the complexity and time-dependent nature of the earthquake-occurrence model required. One method is to calculate hazard probabilities directly from multiple, synthetic-earthquake catalogs according to a particular seismicity model, rather than from the conventional PSHA equations. The seismicity model can be either Poissonian or, in the case of clustering, the Epidemic Type Aftershock Sequence (ETAS) model as proposed by Beauval and others (2006). The Every Earthquake a Precursor According to Scale (EEPAS) model also has been modified to account for clustering in PSHA studies (Rhoades, 2009). Both the ETAS and EEPAS models are tuned according to past seismicity. It is possible to modify these models to develop a PTHA model that includes clustered landslides, although much more data would be needed to tune these models and accommodate the additional PTHA model parameters. Aftershock probabilistic seismic hazard analysis (APSHA) (Yeo and Cornell, 2009) conceivably could be adapted to calculate the hazard from an active landslide region.

Nonstationarity

The occurrence rate of major continental slope landslides appears to be variable and linked to glacial cycles. Lee (2009) indicates that the rate is approximately constant from the last glacial maximum to 5,000 years after the end of the glaciation. Since that time, the rate of major submarine landslides appears to be decreasing. Lee (2009) ascribes the increased rate of major landslides during glaciation to the formation of thick sediment deposits on the upper continental slope and to postglacial rebound seismicity serving as a landslide trigger shortly after glaciation ends. Later in the interglacial cycle it is thought most of the unstable slopes have already failed resulting in lower landslide rates compared to glacial and postglacial times. Considered over the entire glacial cycle, landslide occurrence rates are nonstationary; the source rate-term in PTHA Framework equations is a function of time:

$$\nu_{i=2}(t)\,.$$

Most PTHA applications are designed either for annual probabilities or for time intervals measured in decades (variable T in PTHA Framework). Nonstationarity at time

scales of glacial cycles will not, therefore, significantly affect the PTHA calculation directly. The difficulty, however, is accurately assessing the present-day rate. Using the dates of multiple submarine landslides that span glacial cylces in a particular source region, binning and a curve fitting method would need to be applied to the data in order to estimate the present-day landslide rate. Because of a lack of data in most source regions, present-day rate estimates would be prone to significant uncertainty. The other option is to use age dates from similar type slides over a broad region (or even globally), subject to the ergodic assumption. Even using the ergodic assumption, however, it is questionable whether there is enough data to estimate present-day landslide rates over the past several thousand years. When considering the entire submarine landslide dataset extending back through the last period of glaciation, only landslides under similar glacial environments should be included, so as not to break the ergodic assumption.

Ergodicity

In estimating certain source parameters or their uncertainty, it often is necessary to assume that the physical process (landslide, earthquakes, and other geologic processes) is ergodic. Although the ergodic theorem originating from statistical physics is complex and multifaceted (Anosov, 2001), one important application of the theory is that the time average of a process (x) at a particular geographic point is equal to the average at a particular time (t_0) over an ensemble of points (Beichelt and Fatti, 2002):

$$\lim_{T\to\infty}\frac{1}{2T}\int_{-T}^{T}x(t)dt=\lim_{N\to\infty}\frac{1}{N}\sum_{k=1}^{N}x_k\left(t_0\right)$$

For natural hazards, this allows replacing an estimate of the source or hazard statistics at a particular location where there is limited knowledge throughout time with the statistics of an ensemble of known source or hazard variables over a broad region (or even globally).

An example of where the ergodic assumption is used for earthquakes is estimation of corner moment for a particular fault. Because earthquake catalogs are limited at large magnitudes for a particular fault zone or fault segment throughout time, it is necessary to analyze the statistics of corner moment for a number of faults around the world (Bird and Kagan, 2004). However, Bird and Kagan (2004) note that different types of faults (oceanic transform faults, subduction zones) are separated because of differences in tectonic environment (stress, thermal structure, and so on) (see also Pisarenko and Sornette, 2003). Grouping all subduction zones together, Bird and Kagan (2004) were able to estimate a corner-moment magnitude of 9.58. Even with the expanded catalog of subduction zone earthquakes, however, uncertainty is still difficult to estimate. Bird and Kagan (2004) indicate 95 percent confidence limits of 9.12-? (upper confidence limit not found) using a merged 20th century earthquake catalog and 9.12-10.06 using a seismic-moment conservation argument.

The same type of analysis could be performed to estimate submarine landslide recurrence, although it is unclear what geologic factors are key to defining the ergodic ensemble. If there are multiple dates in a given region where the offshore sediment composition, tectonics, ground shaking, and so on are similar such as in southern

California, the age dates of multiple landslides within in the region can be grouped together to estimate the recurrence of landslides (Lee and others, 2004). For a global ensemble, however, differences in sediment type (clastic vs. carbonate), tectonic movement (passive margin versus active movement as in Puerto Rico), glacial activity, and peak ground acceleration must be taken into account. Too large of an ensemble can result in ergodicity breaking where the assumption no longer applies. This is discussed in the context of estimating uncertainty in the seismic attenuation relationship for earthquake ground motion studies by Anderson and Brune (1999). Lutz (2004) indicates that physical systems that follow Lévy Law distributions may also exhibit ergodicity breaking. Although rigorously proving the ergodic assumption for complex systems is difficult, the assumption should be examined for specific situations to determine its domain of applicability.

Future Science Strategies

There are specific aspects of assessing the hazard of landslide-generated tsunamis that are currently feasible owing to recent research results and discussions held during the NRC/USGS workshop. These aspects include identifying and characterizing significant submarine landslides along U.S. continental margins, although there are critical gaps in multibeam bathymetric coverage that need to be filled in. Care must be taken to avoid false identification of landslides (Lee and others, 2002). In addition, there are cases in which bathymetric evidence of source regions is lacking for past tsunami events in which a significant landslide trigger was thought to be present, suggesting that statistical censoring may be a significant issue in the inventory of significant tsunamigenic landslides. It also is currently feasible to date submarine landslides (Normark and others, 2004). For any given landslide, however, the uncertainty in age dating depends on stratigraphic relationships among failed sediment, characteristics of overlying and underlying strata, and availability of dateable material. More research is needed to refine current capabilities in identifying and dating submarine landslides.

There are a few regions along U.S. continental margins where it may be possible to estimate the recurrence rate for submarine landslides from empirical methods. This requires either a stratigraphic record of past landslides (Fisher and others, 2005; Ryan and others, 2010), or that the ergodic hypothesis is true for a region where there is a sufficient spatial record of landslides. It may be possuble to estimate the probability of occurrence of significant landslides, assuming the landslides occur according to a Poisson process. It also may be possible to infer the rate of submarine landslides from slope stability arguments and the probability of offshore ground shaking (ten Brink and others, 2009c). There is, however, some indication of temporal and spatial clustering and changes in occurrence with glacial cycles (Lee, 2009) that may invalidate a stationary Poisson assumption. Much of the clustering is unquantified, except for well-studied regions, such as Storegga (Haflidason and others, 2004; Haflidason and others, 2005).

There is currently insufficient information with which to incorporate submarine landslides into PTHA at low design probabilities of interest to the NRC. Challenges include dependency among landslide-source parameters, modeling landslide dynamics in relation to tsunami generation, aggregating tidal probabilities with nonlinear tsunami waves, nonstationary landslide rates, temporal and spatial clustering, and whether or not

the ergodic hypothesis holds for landslides and under what conditions. Acquisition of more age dates for submarine landslides along the U.S. continental margins is key to address many of these challenges.

Acknowledgments

The authors appreciate constructive reviews of this workshop report by Rob Kayen and Tom Parsons.

References

Anderson, J.G., and Brune, J.N., 1999, Probabilistic seismic hazard analysis without the ergodic assumption: Seismological Research Letters, v. 70, p. 19-28.

Anosov, D.V., 2001, Ergodic theory, *in* Hazewinkel, M., ed., Encyclopaedia of Mathematics: Berlin, Springer-Verlag, http://eom.springer.de/e/e036150.htm.

Atwater, B.F., Tuttle, M.P., Schweig, E.S., Rubin, C.M., Yamaguchi, D.K., and Hemphill-Haley, E., 2004, Earthquake recurrence inferred from paleoseismology: Developments in Quaternary Science, v. 1, p. 331-350.

Bak, P., Tang, C., and Wiesenfeld, K., 1988, Self-organized criticality: Physical Review A, v. 38, p. 364-374.

Beauval, C., Hainzl, S., and Scherbaum, F., 2006, Probabilistic seismic hazard estimation in low-seismicity regions considering non-Poissonian seismic occurrence: Geophysical Journal International, v. 164, p. 543-550.

Beichelt, F.E., and Fatti, L.P., 2002, Stochastic processes and their applications: London, Taylor and Francis, 326 p.

Bent, A.L., 1995, A complex double-couple source mechanism for the Ms 7.2 1929 Grand Banks earthquake: Bulletin of the Seismological Society of America, v. 85, p. 1003-1020.

Bird, P., and Kagan, Y.Y., 2004, Plate-tectonic analysis of shallow seismicity: Apparent boundary width, beta-value, corner magnitude, coupled lithosphere thickness, and coupling in 7 tectonic settings: Bulletin of the Seismological Society of America, v. 94, p. 2380-2399.

Boore, D.M., and Joyner, W.B., 1997, Site amplifications for generic rock sites: Bulletin of the Seismological Society of America, v. 87, p. 327-341.

Burroughs, S.M., and Tebbens, S.F., 2001, Upper-truncated power laws in natural systems: Pure and Applied Geophysics, v. 158, p. 741-757.

Campbell, K.W., 1982, Bayesian analysis of extreme earthquake occurrences. Part I. Probabilistic hazard model: Bulletin of the Seismological Society of America, v. 72, p. 1689-1705.

Campbell, K.W., 2003, Prediction of strong ground motion using the hybrid empirical method and its use in development of ground-motion (attenuation) relations in Eastern North America: Bulletin of the Seismological Society of America, v. 93, p. 1012-1033.

Chaytor, J.D., ten Brink, U.S., Solow, A.R., and Andrews, B.D., 2009, Size distribution of submarine landslides along the U.S. Atlantic Margin: Marine Geology, p. 16-27.

Cornell, C.A., 1968, Engineering seismic risk analysis: Bulletin of the Seismological Society of America, v. 58, p. 1583-1606.

Coussot, P., 1997, Mudflow rheology and dynamics: Rotterdam, A.A. Balkema, 255 p.

Coussot, P., Laigle, D., Arattano, M., Deganutti, A., and Marchi, L., 1998, Direct determination of rheological characteristics of debris flow: Journal of Hydraulic Engineering, v. 124, p. 865-868.

Coussot, P., and Meunier, M., 1996, Recognition, classification and mechanical description of debris flows: Earth-Science Reviews, v. 40, p. 209-227.

Dai, F.C., and Lee, C.F., 2001, Frequency-volume relation and prediction of rainfall-induced landslides: Engineering Geology, v. 59, p. 253-266.

Densmore, A.L., Ellis, M.A., and Anderson, R.S., 1998, Landsliding and the evolution of normal-fault-bounded mountains: Journal of Geophysical Research, v. 103, p. 15,203-215,219.

Dunning, S.A., Mitchell, W.A., Petley, D.N., Rosser, N.J., and Cox, N.J., 2007, Landslides predating and triggered by the 2005 Kashmir earthquake: Rockfall to rock avalanches: Geophysical Research Abstracts, v. 9, p. 06376.

Dussauge, C., Grasso, J.R., and Helmstetter, A., 2003, Statistical analysis of rockfall volume distributions: Implications for rockfall dynamics: Journal of Geophysical Research, v. 108, p. doi:10.1029/2001JB000650.

Elverhøi, A., Issler, D., De Blasio, F.V., Ilstad, T., Harbitz, C.B., and Gauer, P., 2005, Emerging insights into the dynamics of submarine debris flows: Natural Hazards and Earth System Sciences, v. 5, p. 633-648.

Favre, A.-C., El-Adlouni, S., Perreault, L., Thiémonge, N., and Bobée, B., 2004, Multivariate hydrological frequency analysis using copulas: Water Resources Research, v. 40, p. doi:10.1029/2003WR002456.

Fernández-Nieto, E.D., Bouchut, F., Bresch, D., Castro Diaz, M.J., and Mangeney, A., 2008, A new Savage-Hutter type model for submarine avalanches and generated tsunami: Journal of Computational Physics, v. 227, p. 7720-7754.

Fisher, M.A., Normark, W.R., Greene, H.G., Lee, H.J., and Sliter, R.W., 2005, Geology and tsunamigenic potential of submarine landslides in Santa Barbara Channel, southern California: Marine Geology, v. 224, p. 1-22.

Flinn, E.A., Engdahl, E.R., and Hill, A.R., 1974, Seismic and geographical regionalization: Bulletin of the Seismological Society of America, v. 64, p. 771-992.

Frankel, A.D., Mueller, C.S., Barnhard, T., Perkins, D.M., Leyendecker, E.V., Dickman, N., Hanson, S., and Hopper, M., 1996, National seismic-hazard maps: Documentation June 1996: U.S. Geological Survey Open-File Report 96-532, 41 p.

Geist, E.L., Lynett, P.J., and Chaytor, J.D., 2009a, Hydrodynamic modeling of tsunamis from the Currituck landslide: Marine Geology, v. 264, p. 41-52.

Geist, E.L., and Parsons, T., 2006, Probabilistic analysis of tsunami hazards: Natural Hazards, v. 37, p. 277-314.

Geist, E.L., and Parsons, T., 2010, Estimating the empirical probability of submarine landslide occurrence, *in* Mosher, D.C., Shipp, C., Moscardelli, L., Chaytor, J., Baxter, C., Lee, H.J., and Urgeles, R., eds., Submarine mass movements and their consequences IV: Heidelberg, Germany, Springer, p. 377-386.

Geist, E.L., Parsons, T., ten Brink, U.S., and Lee, H.J., 2009b, Tsunami probability, *in* Bernard, E.N., and Robinson, A.R., eds., The sea, v. 15: Cambridge, Massachusetts, Harvard University Press, p. 93-135.

Genest, C., and Favre, A.-C., 2007, Everthing you always wanted know about copula modeling but were afraid to ask: Journal of Hydraulic Engineering, v. 12, p. 347-368.

González, F.I., Bernard, E.N., Dunbar, P., Geist, E.L., Jaffe, B.E., Kânoglu, U., Locat, J., Mofjeld, H.O., Moore, A., Synolakis, C.E., Titov, V.V., and Weiss, R., 2007, Scientific and technical issues in tsunami hazard assessment of nuclear power plant sites: NOAA Pacific Marine Environmental Laboratory NOAA Technical Memorandum OAR PMEL-136, 125 p.

Gutenberg, B., and Richter, C.F., 1944, Frequency of earthquakes in California: Bulletin of the Seismological Society of America, v. 34, p. 185-188.

Guzzetti, F., Malamud, B.D., Turcotte, D.L., and Reichenbach, P., 2002, Power-law correlations of landslide areas in central Italy: Earth and Planetary Science Letters, v. 195, p. 169-183.

Haflidason, H., Lien, R., Sejrup, H.P., Forsberg, C.F., and Bryn, P., 2005, The dating and morphometry of the Storegga Slide: Marine and Petroleum Geology, v. 22, p. 123-136.

Haflidason, H., Sejrup, H.P., Nygård, A., Mienert, J., Bryn, P., Lien, R., Forsberg, C.F., Berg, K., and Masson, D.G., 2004, The Storegga Slide: Architecture, geometry and slide development: Marine Geology, v. 213, p. 201-234.

Harbitz, C.B., 1992, Model simulations of tsunamis generated by the Storegga slides: Marine Geology, v. 105, p. 1-21.

Harp, E.L., and Wilson, R.C., 1995, Shaking intensity thresholds for rock falls and slides: Evidence from 1987 Whittier Narrows and Superstition Hills earthquake strong-motion records: Bulletin of the Seismological Society of America, v. 85, p. 1739-1757.

Haugen, K.B., Løvholt, F., and Harbitz, C.B., 2005, Fundamental mechanisms for tsunami generation by submarine mass flows in idealised geometries: Marine and Petroleum Geology, v. 22, p. 209-217.

Hergarten, S., 2003, Landslides, sandpiles, and self-organized criticality: Natural Hazards and Earth System Sciences, v. 3, p. 505-514.

Hungr, O., Evans, S.G., Bovis, M.J., and Hutchinson, J.F., 2001, A review of the classification of landslides of the flow type: Environmental and Engineering Geoscience, v. 7, p. 221-238.

Hynes-Griffin, M.E., and Franklin, A.G., 1984, Rationalizing the seismic coefficient method: U.S. Army Engineer Waterways Experiment Station Misc. Paper GL-84-13, 21 p.

Imran, J., Parker, G., Locat, J., and Lee, H., 2001, A 1-D numerical model of muddy subaqueous and subaerial debris flows: Journal of Hydraulic Engineering, v. 127, p. 959-958.

Issler, D., De Blasio, F.V., Elverhøi, A., Bryn, P., and Lien, R., 2005, Scaling behaviour of clay-rich submarine debris flows: Marine and Petroleum Geology, v. 22, p. 187-194.

Iverson, R.M., and Denlinger, R.P., 2001, Flow of variably fluidized granular masses across three-dimensional terrain 1. Coulomb mixture theory: Journal of Geophysical Research, v. 106, p. 537-552.

Jiang, L., and Leblond, P.H., 1993, Numerical modeling of an underwater Bingham plastic mudslide and the waves which it generates: Journal of Geophysical Research, v. 98, p. 10,303-310,317.

Katz, O., and Aharonov, E., 2006, Landslides in a vibrating sand-box: What controls types of slope-failure and frequency magnitude relations?: Earth and Planetary Science Letters, v. 247, p. 280-294.

Keefer, D.K., 1984, Landslides caused by earthquakes: Geological Society of America Bulletin, v. 95, p. 406-421.

Lee, H., Normark, W.R., Fisher, M.A., Greene, H.G., Edwards, B.D., and Locat, J., 2004, Timing and extent of submarine landslides in southern California, *in* Offshore Technology Conference, Houston, Texas, U.S.A., OTC Paper Number 16744.

Lee, H., Syvitski, J.P.M., Parker, G., Orange, D., Locat, J., Hutton, E.W.H., and Imran, J., 2002, Distinguishing sediment waves from slope failure deposits: Field examples including the "Humboldt slide", and modelling results: Marine Geology, v. 192, p. 79-104.

Lee, H.J., 2009, Timing of occurrence of large submarine landslides on the Atlantic ocean margin: Marine Geology, p. 53-64.

Lee, H.J., Locat, J., Dartnell, P., Minasian, D., and Wong, F., 2000, A GIS-based regional analysis of the potential for shallow-seated submarine slope failure, *in* Proceedings of the 8th International Symposium on Landslides, Cardiff, Wales, p. 917-922.

Locat, J., Lee, H., ten Brink, U., Twichell, D., Geist, E.L., and Sansoucy, M., 2009, Geomorphology, stability and mobility of the Currituck slide: Marine Geology, p. 28-40.

Locat, J., and Lee, H.J., 2002, Submarine landslides: advances and challenges: Canadian Geotechnical Journal, v. 39, p. 193-212.

Locat, J., Lee, H.J., Locat, P., and Imran, J., 2004, Numerical analysis of the mobility of the Palos Verdes debris avalanche, California, and its implication for the generation of tsunmis: Marine Geology, v. 203, p. 269-280.

Lutz, E., 2004, Power-law tail distributions and nonergodicity: Physical Review Letters, v. 93, p. doi:10.1103/PhysRevLett.1193.190602.

Lynett, P., and Jimenez, A., 2011, Landslide tsunami hazard assessment approaches, *in* Tsunami Generation by Subaerial/Submarine Landslides Workshop, Texas A&M University, Galveston.

Malamud, B.D., and Turcotte, D.L., 2006, An inverse cascade explanation for the power-law frequency-area statistics of earthquakes, landslides and wildfires, *in* Cello, G., and Malamud, B.D., eds., Fractal Analysis for Natural HAzards: London, Geological Society, Special Publications, p. 1-9.

Malamud, B.D., Turcotte, D.L., Guzzetti, F., and Reichenbach, P., 2004, Landslide inventories and their statistical properties: Earth Surface Processes and Landforms, v. 29, p. 687-7111.

Martel, S.J., 2004, Mechanics of landslide initiation as a shear fracture phenomenon: Marine Geology, v. 203, p. 319-339.

Masson, D.G., Harbitz, C.B., Wynn, R.B., Pedersen, G., and Løvholt, F., 2006, Submarine landslides: Processes, triggers and hazard prediction: Philosophical Transactions of the Royal Society of London, A, v. 364, p. 2009-2039.

Matthews, M.V., Ellsworth, W.L., and Reasenberg, P.A., 2002, A Brownian model for recurrent earthquakes: Bulletin of the Seismological Society of America, v. 92, p. 2233-2250.

Mazzotti, S., and Adams, J., 2005, Rates and uncertainties on seismic moment and deformation in eastern Canada: Journal of Geophysical Research, v. 110, p. doi:10.1029/2004JB003510.

Micallef, A., Berndt, C., Masson, D.G., and Stow, D.A.V., 2008, Scale invariant characteristics of the Storegga Slide and implications for large-scale submarine mass movements: Marine Geology, v. 247, p. 46-60.

Mofjeld, H.O., González, F.I., Titov, V.V., Venturato, A.J., and Newman, A.V., 2007, Effects of tides on maximum tsunami wave heights: Probability distributions: Journal of Atmospheric and Oceanic Technology, v. 24, p. 117-123.

Mofjeld, H.O., Venturato, A.J., González, F.I., and Titov, V.V., 2004, Background tides and sea level variations at Seaside, Oregon: NOAA OAR PMEL-126, 15 p. [Technical Memorandum].

Mortgat, C.P., and Shah, H.C., 1979, A Bayesian model for seismic hazard mapping: Bulletin of the Seismological Society of America, v. 69, p. 1237-1251.

Mosher, D.C., and Piper, D.J.W., 2007, Analysis of multibeam seafloor imagery of the Laurentide Fan and the 1929 Grand Banks landslide area, *in* Lykousis, V.,

Sakellariou, D., and Locat, J., eds., Submarine mass movements and their consequences: Springer, p. 77-88.

Normark, W.R., McGann, M., and Sliter, R.W., 2004, Age of Palos Verdes submarine debris avalanche, southern California: Marine Geology, v. 203, p. 247-259.

Ogata, Y., 1999, Estimating the hazard of rupture using uncertain occurrence times of paleoearthquakes: Journal of Geophysical Research, v. 104, p. 17,995-918,014.

Okal, E.A., and Synolakis, C.E., 2001, Comment on: "Origin of the 17 July 1998 Papua New Guinea tsunami: Earthquake or landslide?" by E.L. Geist: Seismological Research Letters, v. 72, p. 362-366.

Page, M.T., and Carlson, J.M., 2006, Methodologies for earthquake hazard assessment: Model uncertainty and the WGCEP-2002 forecast: Bulletin of the Seismological Society of America, v. 96, p. 1624-1633.

Parsons, T., 2008, Monte Carlo method for determining earthquake recurrence parameters from short paleoseismic catalogs: Example calculations for California: Journal of Geophysical Research, v. 113, p. doi:10.1029/2007JB004998.

Petley, D.N., Higuchi, T., Petley, D.J., Bulmer, M.H., and Carey, J., 2005, Development of progressive landslide failure in cohesive materials: Geology, v. 33, p. 201-204.

Piper, D.J.W., Cochonat, P., and Morrison, M.L., 1999, The sequence of events around the epicentre of the 1929 Grand Banks earthquake: Initiation of debris flows and turbidity current inferred from sidescan sonar: Sedimentology, v. 46, p. 79-97.

Pisarenko, V.F., and Sornette, D., 2003, Characterization of the frequency of extreme earthquake events by the Generalized Pareto Distribution: Pure and Applied Geophysics, v. 160, p. 2343-2364.

Prasad, R., 2009, Tsunami hazard assessment at nuclear power plant sites in the United States of America: U.S. Nuclear Regulatory Commission CR-6966, 117 p.

Pratson, L.F., Ryan, W.B.F., Mountain, G.S., and Twichell, D.C., 1994, Submarine canyon initiation by downslope-eroding sediment flows: Evidence in late Cenozoic strata on the New Jersey continental slope: Geological Society of America Bulletin, v. 106, p. 395-412.

Rhoades, D., 2009, Long-range earthquake forecasting allowing for aftershocks: Geophysical Journal International, v. 178, p. 244-256.

Ryan, H.F., Lee, H.J., Haeussler, P.J., Alexander, C.R., and Kayen, R.E., 2010, Historic and paleo-submarine landslide deposits imaged beneath Port Valdez, Alaska:

Implications for tsunami generation in a glacial fiord, Submarine mass movements and their consequences IV: New York, Springer.

Savage, J.C., 1994, Empirical earthquake probabilities from observed recurrence intervals: Bulletin of the Seismological Society of America, v. 84, p. 219-221.

Scholz, C.H., and Cowie, P.A., 1990, Determination of total strain from faulting using slip measurements: Nature, v. 346, p. 837-839.

Senior Seismic Hazard Analysis Committee, 1997, Recommendations for probabilistic seismic hazard analysis: Guidance on uncertainty and use of experts: U.S. Nuclear Regulatory Commission NUREG/CR-6372 UCRL-ID-122160, v. 1, 256 p. [Main Report].

Sklar, A., 1959, Fonctions de répartition à n dimensions et leurs marges: Publications de l'Institut de Statistique de L'Université de Paris, v. 8, p. 229-231.

Stark, C.P., and Hovius, N., 2001, The characterization of landslide size distributions: Geophysical Research Letters, v. 28, p. 1091-1094.

Stein, S., and Wysession, M., 2003, An introduction to seismology, earthquakes, and Earth structure: Oxford, Blackwell Publishing, 498 p.

Sugai, T., Ohmori, H., and Hirano, M., 1994, Rock control on magnitude-frequency distribution of landslides: Transactions of the Japanese Geomorphological Union, v. 14, p. 233-251.

Talling, P.J., Amy, L.A., and Wynn, R.B., 2007, New insight into the evolution of large-volume turbidity currents: comarison of turbidite shape and previous modeling results: Sedimentology, v. 54, p. 737-769.

ten Brink, U., Twichell, D., Lynett, P., Geist, E.L., Chaytor, J., Lee, H., Buczkowski, B., and Flores, C., 2009a, Regional assessment of tsunami potential in the Gulf of Mexico: Report to the National Tsunami Hazard Mitigation Program: U.S. Geological Survey Administrative Report, 90 p.

ten Brink, U.S., Barkan, R., Andrews, B.D., and Chaytor, J.D., 2009b, Size distributions and failure initiation of submarine and subaerial landslides: Earth and Planetary Science Letters, v. 287, p. 31-42.

ten Brink, U.S., Geist, E.L., and Andrews, B.D., 2006a, Size distribution of submarine landslides and its implication to tsunami hazard in Puerto Rico: Geophysical Research Letters, v. 33, p. doi:10.1029/2006GL026125.

ten Brink, U.S., Geist, E.L., Lynett, P.J., and Andrews, B.D., 2006b, Submarine slides north of Puerto Rico and their tsunami potential, *in* Mercado, A., and Liu, P., eds., Caribbean tsunami hazard: Singapore, World Scientific, p. 67-90.

ten Brink, U.S., Lee, H.J., Geist, E.L., and Twichell, D., 2009c, Assessment of tsunami hazard to the U.S. Atlantic Coast using relationships between submarine landslides and earthquakes: Marine Geology, v. 264, p. 65-73.

Tripsanas, E.K., Piper, D.J.W., and Campbell, D.C., 2008, Evolution and depositional structure of earthquake-induced mass movements and gravity flows: Southwest Orphan Basin, Labrador Sea: Marine and Petroleum Geology, v. 25, p. 645-662.

Turcotte, D.L., and Malamud, B.D., 2004, Landslides, forest fires, and earthquakes: Examples of self-organized critical behaviour: Physica A, v. 340, p. 580-589.

Twichell, D., Chaytor, J.D., ten Brink, U.S., and Buczkowski, B., 2009, Morphology of late Quaternary submarine landslides along the U.S. Atlantic continental margin: Marine Geology, v. 264, p. 4-15.

Varnes, D.J., 1978, Slope movement types and processes, *in* Schuster, R.L., and Krizek, R.J., eds., Landslides: Analysis and control: Washington, D.C., National Academy of Sciences, p. 11-33.

Ward, S.N., 2001, Landslide tsunami: Journal of Geophysical Research, v. 106, p. 11,201-211,215.

Wells, D.L., and Coppersmith, K.J., 1994, New empirical relationships among magnitude, rupture length, rupture width, rupture area, and surface displacement: Bulletin of the Seismological Society of America, v. 84, p. 974-1002.

Yeo, G.L., and Cornell, C.A., 2009, A probabilistic framework for quantification of aftershock ground-motion hazard in California: Methodology and parametric study: Earthquake Engineering and Structural Dynamics, v. 38, p. 45-60.

Appendix

Agenda

Thursday Morning Session: Landslide Geometry & Recurrence

8:30 Coffee/Breakfast & Registration

9:00 Welcome (*Walter Barnhardt, Woods Hole Science Center Director*)
9:05 Logistics, Introductions, Workshop Objectives (*Uri ten Brink and Eric Geist*)
9:10 NRC perspective (*Annie Kammerer*)

9:15 Identifying Submarine Landslides & Their Timing (*Homa Lee*)

10:00 Overview of Atlantic & Gulf of Mexico Landslides (*David Twichell*)

10:45 Coffee break

11:00 Determining the Age and Recurrence Time of Submarine Landslides: Successes and Challenges (*Jason Chaytor*)

11:45 Sediment Transport Processes Associated with Landslides (*Danny Brothers*)

Thursday Afternoon Session: Landslide Mechanics

1:30 Landslide Initiation**:** Earthquakes and Landslides (*Uri ten Brink*)

2:15 Best Practice Recommendations for Geotechnical Site Characterization of Cohesive Offshore Sediments (*Don DeGroot*)

3:00 Coffee break

3:15 Geomorphological and Geotechnical Considerations Towards Tsunamigenic Submarine Slide Risk Assessment (*Jacques Locat*)

4:00 Modeling Tsunamigenic Landslides with Shallow-Flow Equations (*David George*)

Friday Morning Session: Modeling Landslide Tsunamis

8:30 Coffee/Breakfast

8:40 Welcome (*Eric Geist*)

8:45 Landslide Tsunami Generation (3D) and Propagation (2D) (*Juan Horrillo*)

9:30 Recent modeling Work for Landslide Tsunami Generation and Propagation (*Stéphan Grilli*)

10:15 Coffee break

10:30 Probabilistic Assessment of the Tsunami Induced by a Submarine Landslide (*Pat Lynett*)

Friday Session: Probability of Landslides and Landslide Tsunamis

11:15 PTHA Based on PSHA: Methodology and Applications (*Frank González*)

1:00 Probabilistic Tsunami Hazard Analysis (*Hong Kie Thio*)

1:45 Proposed Methodology for a Probabilistic Tsunami Hazard Assessment from Submarine Mass Failures on the U.S. East Coast (*Chris Baxter*)

2:30 Coffee break

2:45 Mapping the Probability of Earthquake-Induced Submarine Slope Failure Along the U.S. Atlantic Margin: A First-Order, Second-Moment Approach (*Eugene Morgan*)

3:30 Summary: Approaches & Challenges of Incorporating Submarine Landslides into PTHA (*Eric Geist*)

4:15 Feedback and Discussion with NRC (*Henry Jones and Annie Kammerer*)

4:45 Wrap-up: Identifying Gaps in Observations and Theory (*Eric Geist and Uri ten Brink*)

Abstracts and Presentations

Workshop presentations and abstracts written by the presenters are given in the order indicated in the agenda below.

Timelines of USGS – NRC tsunami work

Dec. 24, 2004 Sumatra earthquake and tsunami

2006 - 2007 Report on the current state of knowledge regarding potential tsunami sources affecting the U.S. East and Gulf Coasts (Summary of current knowledge)

2007 - 2010 Potential tsunami sources affecting the U.S. Atlantic and Gulf of Mexico coasts (Original work resulting in a 300 pp. report and 9 peer-reviewed papers. Main conclusion: Most significant tsunami hazard is from submarine landslides)

2008 - As needed, provide advise to the Office of New Reactors regarding applications for new power plants (6 applications to date)

Mar. 11, 2011 Tohoku earthquake and tsunami

2010 - 2014 Tsunami source probability and impact on new and existing power plants

Workshop on Landslide tsunami probability
Woods Hole, MA, August 18-19

Goal of the workshop

Bring together experts who study the geometry and recurrence of slope failures, their geotechnical properties, their potential tsunami generation, and the probability of recurrence of extreme events, to answer the following questions:

A) What can we say about the probability for submarine mass failures with the data we currently have?

B) How do we treat the dynamics of landslide movement probabilistically?

C) How do we treat propagation and runup of tsunami waves probabilistically?

D) What new probabilistic methods can be developed specifically for submarine mass failures?

Although probability is mentioned in all of these questions, a probabilistic assessment is only as good as the underlying data and assumptions. Therefore, it is critical that we address the state of knowledge and the kinds of new data needs to be collected to improve our ability to estimate probability of occurrence.

Agenda - continued

Thursday Morning Session: Landslide Geometry & Recurrence

9:15 Identifying Submarine Landslides & Their Timing (*Homa Lee*)

10:00 Overview of Atlantic & Gulf of Mexico Landslides (*David Twichell*)

10:45 Coffee break

11:00 Determining the Age and Recurrence Time of Submarine Landslides: Successes and Challenges (*Jason Chaytor*)

11:45 Sediment Transport Processes Associated with Landslides (*Danny Brothers, given by Uri ten Brink*)

Informal Lunch at the buttery (*12:30-1:30*)

Thursday Afternoon Session: Landslide Mechanics

1:30 Landslide Initiation**:** Earthquakes and Landslides (*Uri ten Brink*)

2:15 Best Practice Recommendations for Geotechnical Site Characterization of Cohesive Offshore Sediments (*Don DeGroot*)

3:00 Coffee break

3:15 Geomorphological and Geotechnical Considerations Towards Tsunamigenic Submarine Slide Risk Assessment (*Jacques Locat*)

4:00 Modeling Tsunamigenic Landslides with Shallow-Flow Equations (*David George*)

Italian Dinner in Falmouth (*Thursday Evening*)

Agenda - continued

Friday Morning Session: Modeling Landslide Tsunamis

8:30 Coffee/Breakfast

8:40 Welcome (*Eric Geist*)

8:45 Landslide Tsunami Generation (3D) and Propagation (2D) (*Juan Horillo*)

9:30 Recent modeling Work for Landslide Tsunami Generation and Propagation (*Stéphan Grilli*)

10:15 Coffee break

10:30 Probabilistic Assessment of the Tsunami Induced by a Submarine Landslide (*Pat Lynett*)

Friday Session: Probability of Landslides and Landslide Tsunamis

11:15 PTHA Based on PSHA: Methodology and Applications (*Frank González*)

Informal Lunch at the Buttery (*12:00-1:00*)

1:00 Probabilistic Tsunami Hazard Analysis (*Hong Kie Thio*)

1:45 Proposed Methodology for a Probabilistic Tsunami Hazard Assessment from Submarine Mass Failures on the U.S. East Coast (*Chris Baxter*)

2:30 Coffee break

2:45 Mapping the Probability of Earthquake-Induced Submarine Slope Failure Along the U.S. Atlantic Margin: A First-Order, Second-Moment Approach (*Eugene Morgan*)

3:30 Summary: Approaches & Challenges of Incorporating Submarine Landslides into PTHA (*Eric Geist*)

4:15 Feedback and Discussion with NRC (*Henry Jones, Annie Kammerer, Richard Raione*)

4:45 Wrap-up: Identifying Gaps in Observations and Theory (*Eric Geist and Uri ten Brink*)